Article

Cell Host & Microbe

Immunoglobulin A controls intestinal virus colonization to preserve immune homeostasis

Graphical abstract

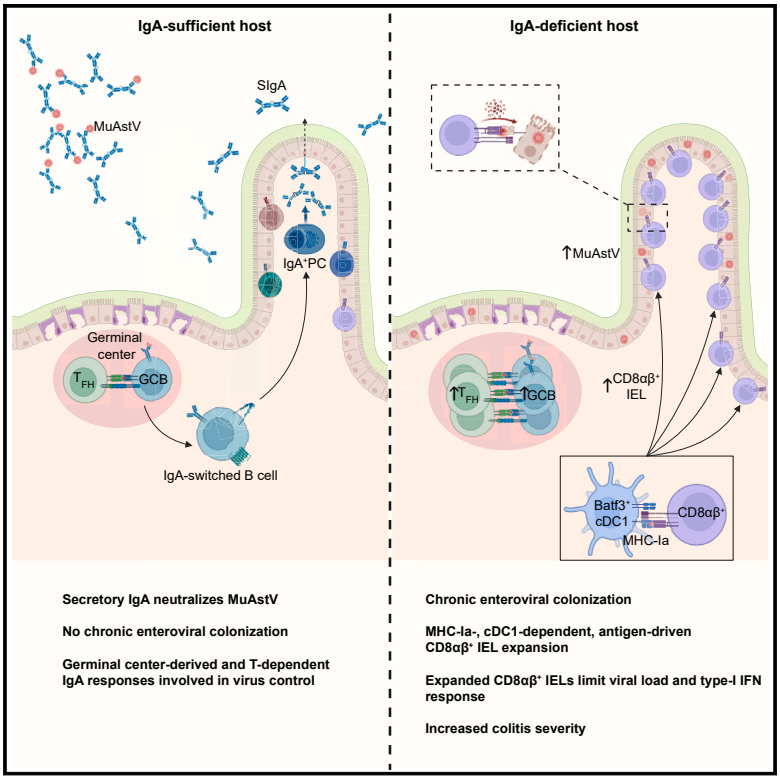

Highlights

- Secretory IgA neutralizes enteric viruses to prevent chronic colonization
- Germinal center-derived and T cell-dependent IgA restricts viral colonization
- Antigen-driven CD8αβ+ IELs in IgA-deficient mice partially control the viral load
- Chronic viral colonization in IgA-deficient hosts exacerbates colitis outcomes

Authors

Wioletta Lisicka, Zachary M. Earley, Joseph J. Sifakis, ..., Samantha J. Riesenfeld, Albert Bendelac, Bana Jabri

Correspondence

bjabri@bsd.uchicago.edu

In brief

Germinal center-derived, T cell-dependent secretory IgA prevents chronic intestinal colonization by select enteroviruses. In its absence, antigen-driven CD8αβ+ intraepithelial lymphocytes partially control viral load and reduce type I IFN responses. The presence of select enteric viruses in IgA-deficient hosts exacerbates colitis when secondary genetic or environmental colitogenic factors are present.

Lisicka et al., 2025, Cell Host & Microbe *33*, 498–511
April 9, 2025
https://doi.org/10.1016/j.chom.2025.03.004

CellPress

CellPress

Cell Host & Microbe

Article

Immunoglobulin A controls intestinal virus colonization to preserve immune homeostasis

Wioletta Lisicka,[1,2,12] Zachary M. Earley,[1,2,8,12] Joseph J. Sifakis,[4] Steven A. Erickson,[1,3,14] Jonathan R. Mattingly,[1,3] Natalie J. Wu-Woods,[5] Siddharth R. Krishnamurthy,[7] Yasmine Belkaid,[7] Rustem F. Ismagilov,[5,6] Jason G. Cyster,[8] Samantha J. Riesenfeld,[1,2,9,10] Albert Bendelac,[1,3,12,13] and Bana Jabri[1,2,3,11,12,15,*]

[1]Committee on Immunology, University of Chicago, Chicago, IL, USA
[2]Department of Medicine, University of Chicago, Chicago, IL, USA
[3]Department of Pathology, University of Chicago, Chicago, IL, USA
[4]Department of Chemistry, University of Chicago, Chicago, IL, USA
[5]Division of Chemistry and Chemical Engineering, California Institute of Technology, Pasadena, CA, USA
[6]Division of Biology and Biological Engineering, California Institute of Technology, Pasadena, CA, USA
[7]Metaorganism Immunity Section, Laboratory of Host Immunity and Microbiome, National Institute of Allergy and Infectious Diseases, National Institutes of Health, Bethesda, MD, USA
[8]Department of Microbiology and Immunology, University of California, San Francisco, San Francisco, CA, USA
[9]Institute for Biophysical Dynamics, University of Chicago, Chicago, IL, USA
[10]Pritzker School of Molecular Engineering, University of Chicago, Chicago, IL, USA
[11]Paris City University, Imagine Institute, Paris, France
[12]These authors contributed equally
[13]Deceased
[14]Present address: Yale School of Medicine, New Haven, CT, USA
[15]Lead contact
*Correspondence: bjabri@bsd.uchicago.edu
https://doi.org/10.1016/j.chom.2025.03.004

SUMMARY

Immunoglobulin A (IgA) is the predominant immunoglobulin isotype in mammals, primarily secreted at type I mucosal surfaces. Despite its abundance, the precise role of secretory IgA in the intestinal lumen, where it coats a diverse array of commensal microbiota, has remained elusive. Our study reveals that germinal center IgA responses are essential for preventing chronic colonization of the gut by specific viruses. In the absence of IgA, chronic viral colonization triggers an antigen-driven expansion of CD8$\alpha\beta^+$ intraepithelial lymphocytes (IELs). Although these IELs are unable to clear the virus, they contribute to maintaining homeostasis by regulating its load and type I interferon responses. Consequently, IgA deficiency increases susceptibility to colitis in genetically susceptible hosts or following chemical induction but only in the presence of viral pathobionts requiring IgA for their clearance. These findings underscore the potential vulnerability of IgA-deficient individuals to immunopathology when exposed to selective viral pathobionts.

INTRODUCTION

The mucosal barrier of the gastrointestinal tract is essential for maintaining tolerance to the commensal microbiota and protecting the host from pathogenic infections. A vital component of this barrier is secretory immunoglobulin A (SIgA), which coats up to 70% of the microbiota in the small intestine[1] and represents the most abundant antibody isotype produced in the mammalian gastrointestinal mucosa.[2] IgA deficiency is one of the most common primary immunodeficiencies, occurring at frequencies ranging from 1 in 300 to 1 in 18,500 in various populations.[3] While most IgA-deficient individuals are asymptomatic, some reports link IgA deficiency to increased susceptibility to infections[4,5] and autoimmune diseases in humans.[3,6,7] Studies in mice suggest that SIgA may both restrict colonization by the adherent commensal segmented filamentous bacteria (SFB)[8,9] and promote mucosal bacterial colonization.[10] Additional studies suggest that SIgA regulates bacterial gene expression and metabolism,[11–13] confers protection against mucosal infections,[14–17] and neutralizes toxins.[18,19] Together, these observations support a role for SIgA in regulating host-bacterial interactions at mucosal surfaces. While IgA deficiencies have been associated with increased viral infections in humans, no experimental evidence has demonstrated that IgA directly regulates viral colonization to ensure immune homeostasis.

Confounding interpretations of IgA function are potential IgM compensation. IgM is a pentameric immunoglobulin covalently associated with the joining chain (J-chain); thus, it can be

transported to the intestinal lumen by polymeric Ig receptor (pIgR). IgM was reported to coat intestinal microbes in AID-deficient mice[1] and IgA-deficient humans.[20] These data point to a hypothesis that IgM may compensate for and control the microbiota in conditions of IgA deficiency. Analogous to IgA-deficient patients,[21,22] the original IgA-deficient mouse model (*Igha*$^{-/-}$) exhibits an increase of serum and mucosal IgM.[23] This emphasizes the need for a model of IgA deficiency devoid of increased IgM responses to assess the function of IgA.

To gain insights into how IgA deficiency may disrupt immune homeostasis, we designed a unique mouse model of IgA deficiency devoid of compensatory hyper-IgM production by enabling class switching to IgA but preventing its secretion through deletion of the secretory tailpiece. Our study sheds light on the specific interactions between IgA and the gut virome, which are crucial for maintaining intestinal immune homeostasis and preventing immunopathology.

RESULTS

IgA-mediated regulation of the microbiota prevents antigen-driven expansion of CD8αβ$^+$ IELs

To evaluate the contribution of IgA in preserving intestinal immune homeostasis without compensatory IgM production, we established a mouse model of IgA deficiency termed *Ighasec*$^{-/-}$. This was achieved by deleting the secretory tailpiece along with its downstream polyadenylation (poly(A)) sites (Figure S1A). Unlike in the original IgA-deficient mice (*Igha*$^{-/-}$), which lack IgSα + IgCα1, *Ighasec*$^{-/-}$ B cells retain the ability to class switch and express IgA on the cell surface as observed in the Peyer's patches (PPs) (Figure S1B). These IgA-switched B cells are incapable of maturing into IgA plasma cells (PCs) within the intestinal lamina propria (LP), resulting in an inability to secrete IgA (Figure S1C). This deficiency leads to decreased levels of both serum and bacterial-bound IgA (Figures S1D and S1E). Of note, while *Ighasec*$^{-/-}$ mice display normal numbers of IgA-switched cells in the PPs (Figure S1B), the numbers of IgA$^+$ PCs were significantly reduced in the lamina propria (Figure S1C). The reduction in IgA$^+$ PC numbers may be driven by increased endoplasmic reticulum (ER) stress, arising from impaired IgA secretion caused by the deletion of the secretory tail piece in *Ighasec*$^{-/-}$ mice. This proposed mechanism is consistent with a recent study[24] showing that conditional deletion of *Sec22b* in B cells—an essential factor in protein secretion—leads to early PC loss and increased apoptosis during PC differentiation. Furthermore, although we were unable to detect IgM-bacterial coating in either *Igha*$^{-/-}$ or *Ighasec*$^{-/-}$ mice (Figure S1E), *Igha*$^{-/-}$ mice had a near 100-fold expansion of IgM PCs and a 3-fold increase in serum IgM, which was absent in the *Ighasec*$^{-/-}$ mice (Figures S1F–S1H). We therefore used the *Ighasec*$^{-/-}$ mice for all subsequent experiments to study IgA deficiency in the absence of potential IgM compensation, unless stated otherwise. *Ighasec*$^{-/-}$ mice showed a 50-fold increase in the number of intraepithelial CD8αβ$^+$ T cells throughout the small intestine compared with littermate control *Ighasec*$^{+/-}$ mice (Figures 1A and 1B). By contrast, the number of unconventional T cell subsets, TCRαβ$^+$ CD8αα$^+$ or TCRγδ$^+$ cells, or the conventional TCRαβ$^+$CD4$^+$ intraepithelial lymphocytes (IELs) remained unchanged (Figure S1I). Expansion of the CD8αβ$^+$ IELs occurred after weaning and was long-lived, persisting in up to 48-week-old *Ighasec*$^{-/-}$ hosts (Figure 1C). Furthermore, intracellular flow cytometry staining revealed increased interferon (IFN)γ production by CD8αβ$^+$ IELs in *Ighasec*$^{-/-}$ mice (Figure 1D). It is noteworthy that the expansion of CD8αβ$^+$ T cells was also evident in mice lacking B cells (*JH*$^{-/-}$) and in *Igha*$^{-/-}$ mice housed in the same facility as *Ighasec*$^{-/-}$ mice (Figures 1E and 1F), suggesting that IgM does not compensate to prevent the expansion of CD8αβ$^+$ IELs in multiple mouse models with IgA deficiency.

We next sought to better understand the mechanisms underlying the expansion of CD8αβ$^+$ IELs. CD4 T cell depletion revealed that the expansion of CD8αβ$^+$ IELs in *Ighasec*$^{-/-}$ was CD4 T cell-dependent (Figure S1J). Since the BATF3-dependent cDC1 dendritic cell lineage[25] is important for cross-presenting viral, bacterial, and tumor antigens to activate CD8αβ T cells,[25,26] we generated *Ighasec*$^{-/-}$*Batf3*$^{-/-}$ mice. The expansion of CD8αβ$^+$ IELs was absent in these mice (Figure 1G), suggesting a role of cDC1s in priming this response.

Next, we aimed to determine the major histocompatibility complex (MHC) molecule through which the expanded CD8αβ$^+$ IELs in *Ighasec*$^{-/-}$ mice are restricted. β_2-microglobulin (β_2M) is an adaptor molecule capable of binding to classical MHCIa and numerous non-classical MHCIb molecules.[27] *Ighasec*$^{-/-}$*B2m*$^{-/-}$ mice had no detectable CD8αβ$^+$ IELs (Figure 1H). To determine whether the CD8αβ$^+$ IELs are classically MHCI restricted, we generated *Ighasec*$^{-/-}$*K*^{b}*D*$^{b-/-}$ triple-deficient mice lacking both MHCIa alleles. There was a significant reduction in CD8αβ$^+$ IELs in *Ighasec*$^{-/-}$*K*^{b}*D*$^{b-/-}$ compared with *Ighasec*$^{-/-}$*K*^{b}*D*$^{b+/-}$ littermate controls (Figure 1I), highlighting the significant contribution of classically restricted CD8αβ$^+$ T cells to the expansion of IELs in IgA-deficient mice. However, in the absence of classical MHCIa molecules, IgA deficiency was still associated with a higher number of IELs (Figure S1K). Therefore, we cannot exclude the possibility that β_2M-dependent, non-classical MHC molecules such as Qa1 may drive the expansion of IELs. Lastly, given that IgA coats the microbiota, we hypothesized that the expansion of CD8αβ$^+$ IELs was microbiota dependent. Consistent with this hypothesis, in germ-free (GF) *Ighasec*$^{-/-}$ mice, CD8αβ$^+$ IELs failed to expand or increase IFNγ production (Figures 1J and 1K).

We then jointly analyzed the T cell receptor (TCR) repertoire and gene expression of CD8αβ$^+$ IELs in *Ighasec*$^{-/-}$ mice using 10× 5′ single-cell RNA sequencing (scRNA-seq) with immune repertoire profiling and found evidence of antigen-driven expansion (Figure 2A). Further analysis of the scRNA-seq data showed that these expanded clones were predominantly present in a few clusters (clusters 0, 2, and 4) (Figures 2B and 2C), which exhibited relatively high expression of either T cell activation markers (*Cd69*, *Ifng*, and *Nr4a1*) or cytotoxicity-associated genes (*Gzmb* and *Gzma*) (Figure 2D). Some of these expanded clones shared specific motifs in complementarity-determining region 3 (CDR3) that were observed across multiple IgA-deficient hosts but rarely in control mice (Figure 2E). These data further support the notion that CD8αβ$^+$ IELs expand in response to antigens presented by classical MHC class I molecules on BATF3$^+$ DCs.

Taken together, these results demonstrate that in the absence of IgA, there is a microbiota-dependent classical adaptive CD8αβ$^+$ IEL immune response driven by cDC1s.

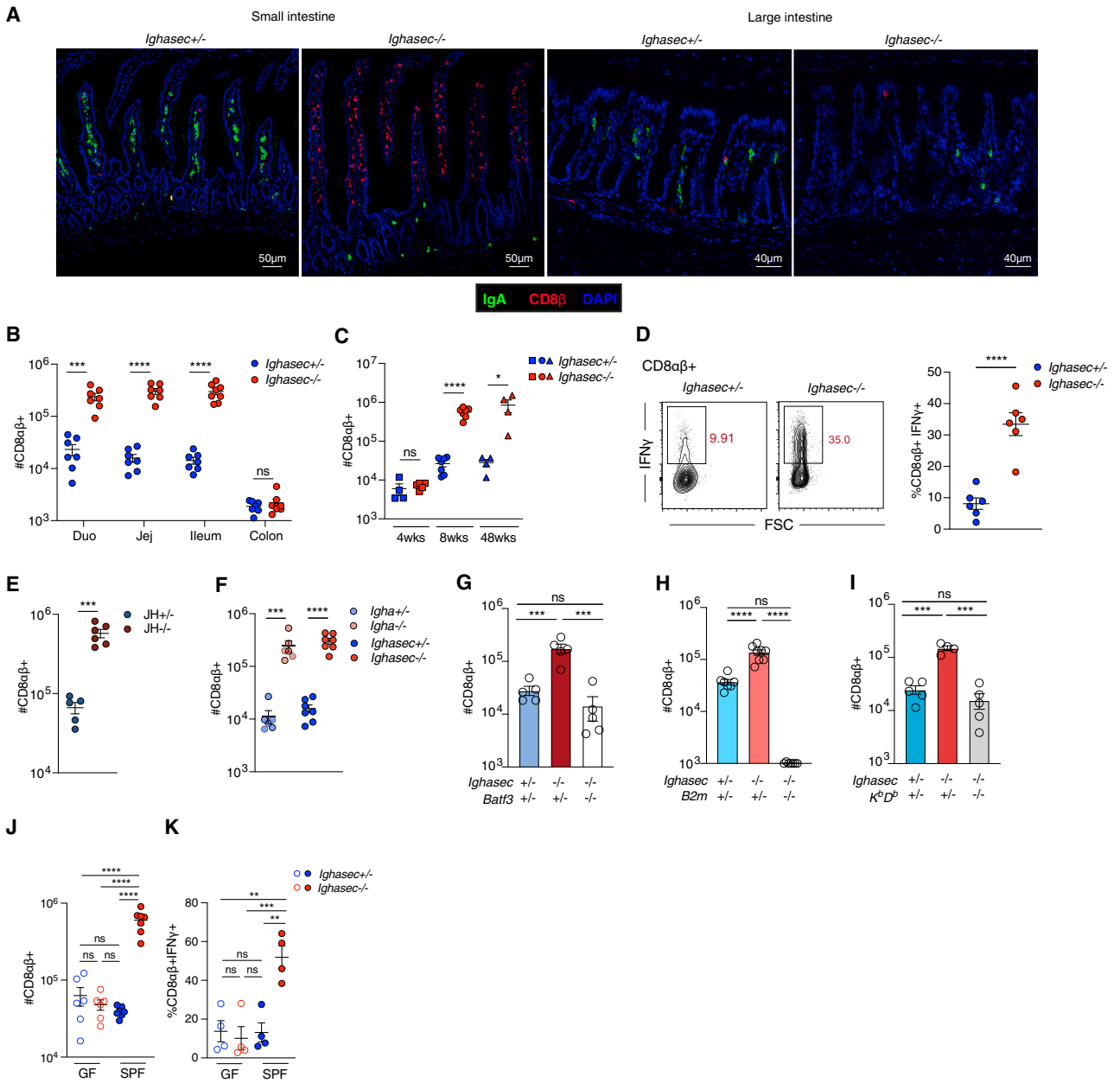

Figure 1. IgA controls microbiota to prevent the expansion of classically restricted CD8αβ$^+$ IELs

(A) Immunofluorescence staining of small and large intestinal tissue using anti-IgA antibody (green), anti-CD8β antibody (red), and counterstained with DAPI (blue). Figure is a representative image from 4 independent *Ighasec*$^{+/-}$ and *Ighasec*$^{-/-}$ animals.

(B) Number of CD8αβ$^+$ IELs in each intestinal segment of *Ighasec*$^{+/-}$ and *Ighasec*$^{-/-}$ mice. $n = 7$ mice/group.

(C) Number of CD8αβ$^+$ IELs in the jejunum of 4-, 8-, and 48-week-old *Ighasec*$^{+/-}$ and *Ighasec*$^{-/-}$ mice. $n = 4$–7 mice/group.

(D) Representative (left) and summary (right) plots of the frequencies of IFN-γ$^+$ cells among CD8αβ$^+$ IELs from the jejunum of *Ighasec*$^{+/-}$ and *Ighasec*$^{-/-}$ mice. $n = 6$ mice/group.

(E and F) Number of CD8αβ$^+$ IELs in the jejunum of *JH*$^{+/-}$ and *JH*$^{-/-}$ (E) or *Igha*$^{+/-}$ and *Igha*$^{-/-}$ or *Ighasec*$^{+/-}$ and *Ighasec*$^{-/-}$ mice (F). $n = 5$–6 mice/group.

(G, H, and I) Number of CD8αβ$^+$ IELs in the jejunum of *Ighasec*$^{+/-}$*Batf3*$^{+/-}$, *Ighasec*$^{-/-}$*Batf3*$^{+/-}$, and *Ighasec*$^{-/-}$*Batf3*$^{-/-}$ mice (G); *Ighasec*$^{+/-}$*B2m*$^{+/-}$, *Ighasec*$^{-/-}$*B2m*$^{+/-}$, and *Ighasec*$^{-/-}$*B2m*$^{-/-}$ mice (H); and *Ighasec*$^{+/-}$*K*^{b}*D*$^{b+/-}$, *Ighasec*$^{-/-}$*K*^{b}*D*$^{b+/-}$, and *Ighasec*$^{-/-}$*K*^{b}*D*$^{b-/-}$ mice (I). $n = 4$–8 mice/group.

(J and K) Number of CD8αβ$^+$ IELs (J) and the frequency of IFN-γ$^+$ cells among CD8αβ$^+$ IELs (K) in the jejunum of GF and SPF *Ighasec*$^{+/-}$ and *Ighasec*$^{-/-}$ mice. $n = 4$–7 mice/group.

All data in this figure are pooled from at least two independent experiments and are represented as mean or mean ± SEM. $^{****}p < 0.0001$, $^{***}p < 0.001$, $^{**}p < 0.01$, $^{*}p < 0.05$, ns $p \geq 0.05$. Unpaired t test (B–F, J, and K), ANOVA with Tukey multiple comparison test (G–I).

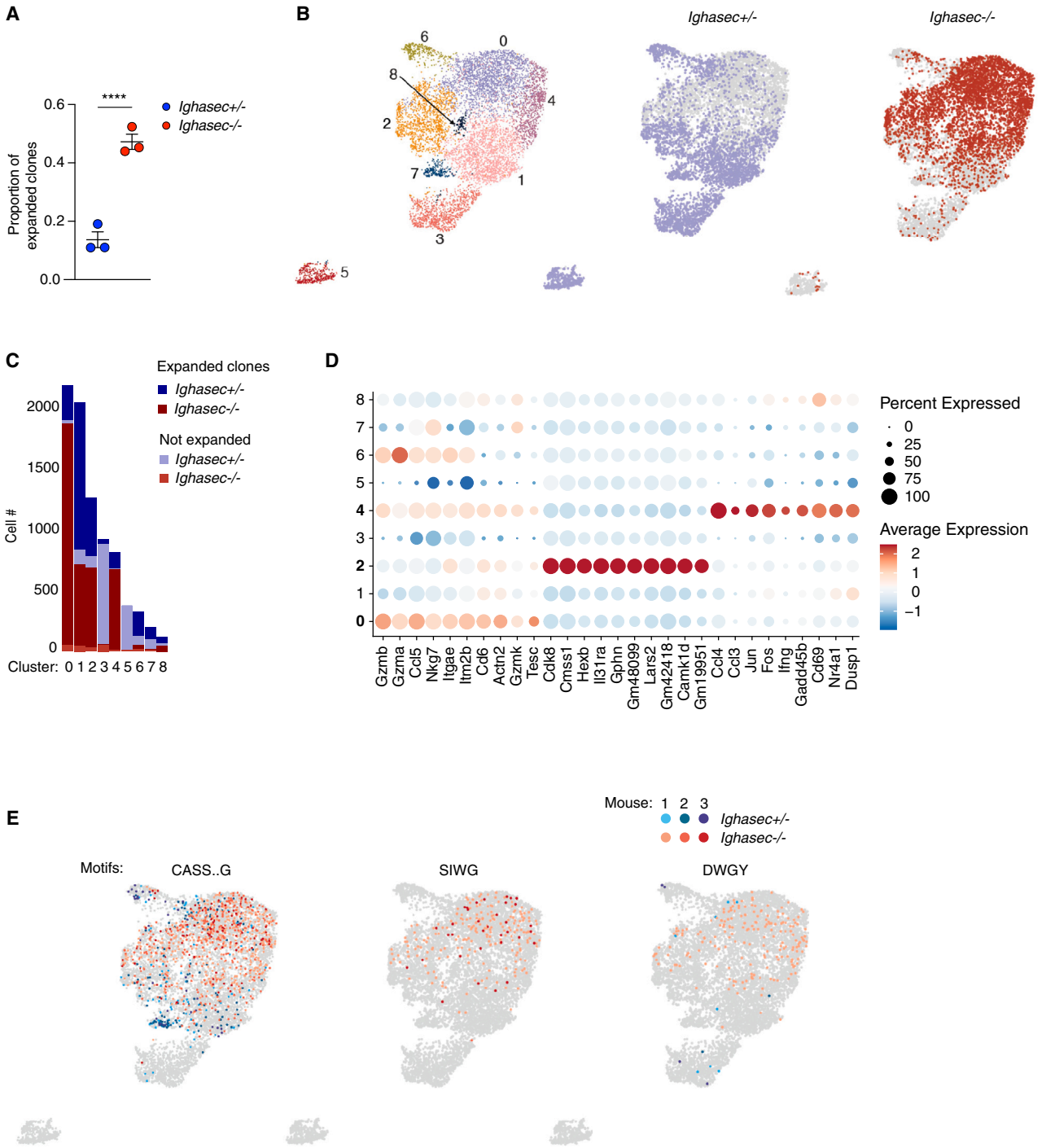

Figure 2. IgA deficiency leads to antigen-driven expansion of CD8αβ$^+$ IELs

(A) Proportion of expanded clones among CD8αβ$^+$ IELs from the jejunum of *Ighasec*$^{+/-}$ and *Ighasec*$^{-/-}$ mice. Expanded clones were defined as unique TCRs that were expressed by at least 2 cells. $n = 3$ mice/group.

(B) Uniform manifold approximation projection (UMAP) embedding of scRNA-seq profiles of CD8αβ$^+$ IELs from the jejunum of *Ighasec*$^{+/-}$ and *Ighasec*$^{-/-}$ mice, colored by cluster (left) and mouse genotype (right).

(C) Bar chart representing the number of expanded or unique CD8αβ$^+$ IEL clones in each transcriptional cluster (as in B).

(D) Dot plot representing expression (color) in clusters (rows) of top differentially expressed genes (columns) in CD8αβ$^+$ IELs from the jejunum of *Ighasec*$^{+/-}$ and *Ighasec*$^{-/-}$ mice. Dot color: normalized expression. Dot size: percent of cells in cluster expressing the gene.

(legend continued on next page)

IgA prevents MuAstV expansion in the small intestine

To determine whether specific microbes induced the expansion of intraepithelial CD8αβ$^+$ IELs in the small intestine of IgA-deficient animals, we transplanted GF mice with limited consortia or complete microbiota from distinct animal facilities. Specifically, GF *Ighasec*$^{+/-}$ and *Ighasec*$^{-/-}$ mice were transplanted with fecal microbiota from five different sources: (1) University of Chicago SPF Barrier I room (SFB$^+$, *Helicobacter* spp$^+$, and murine norovirus [MNV]$^+$), (2) the University of Chicago SPF Barrier II room (SFB$^-$, *Helicobacter* spp$^-$, and MNV$^-$), (3) C57BL/6J mice from Jackson laboratory (JAX), (4) altered Schaedler flora (ASF), and (5) a 13-species consortium. Limited consortia of microbes failed to induce expansion of CD8αβ$^+$ IELs in *Ighasec*$^{-/-}$ recipients. By contrast, complex microbiota present in the mice at UofC Barrier I and II, and JAX microbiota led to the expansion (Figure 3A). These data, along with the observation that the CD8αβ+ IELs were clonally expanded (Figures 2A–2C and 2E), suggest that IgA regulates specific commensal microbes to restrain inflammatory CD8αβ$^+$ T cell responses in the small intestine. While conducting our studies, we serendipitously identified a single litter of *Ighasec*$^{-/-}$ mice in UofC Barrier II that had low numbers of CD8αβ$^+$ T cells (Figure 3B). We propagated the mice from the CD8αβ$^+$ low litter and found that the progeny maintained the low CD8αβ$^+$ phenotype, further supporting the hypothesis that expansion of intraepithelial CD8αβ$^+$ T cells in IgA-deficient mice was associated with distinct microbiota.

To identify microbes driving inflammatory T cell responses in IgA-deficient hosts, we performed 16S rRNA gene sequencing of intestinal luminal contents. We utilized animals from UofC Barrier II (*Hpp*$^-$, MNV$^-$, and SFB$^-$) for the 16S rRNA gene sequencing since *Ighasec*$^{-/-}$ mice housed in this facility exhibited the CD8αβ$^+$ T cell expansion but lacked microbes, such as SFB, known to be regulated by IgA.[8,9] We sequenced intestinal luminal contents from each segment of co-housed *Ighasec*$^{+/-}$ and *Ighasec*$^{-/-}$ mice, as well as CD8αβ-low versus CD8αβ-high *Ighasec*$^{-/-}$ litters. The analysis of the bacterial communities in the small intestines of *Ighasec*$^{+/-}$ mice, compared with those of *Ighasec*$^{-/-}$ mice, revealed no significant differences in either relative or absolute genera abundances (Figure S2A). In addition, we did not find any bacterial taxa that segregated with the CD8αβ high phenotype (Figure S2B).

To further investigate which IgA-controlled microbe may be driving the expansion of CD8αβ$^+$ IELs, we performed a limiting dilution fecal microbiota transfer. First, we aimed to reduce microbiota diversity via antibiotic treatment. 4-week treatment with vancomycin (V) and metronidazole (M) did not reduce the CD8αβ$^+$ T cell expansion in *Ighasec*$^{-/-}$ hosts, suggesting the microbe was V/M resistant (Figure S2C). We confirmed that fecal microbiota transfer from V/M-treated *Ighasec*$^{-/-}$ mice to GF mice was sufficient to induce CD8αβ$^+$ T cell expansion (Figure S2D). Next, we performed serial dilutions of V/M *Ighasec*$^{-/-}$ feces and transferred them to GF mice (Figure S2E). 4 weeks post transfer, we observed the expansion of intraepithelial CD8αβ$^+$ IELs in *Ighasec*$^{-/-}$ recipients of 10^4-fold diluted fecal material (Figure S2F). Metagenomic sequencing of the fecal content revealed that 99.8% of filtered bacterial reads (4,274,184 out of 4,284,095) were mapped to *Limosilactobacillus reuteri* (Figure S2G). Furthermore, microbial profiling with MetaPhlAn, which utilizes unique clade-specific marker genes, identified *L. reuteri* as the only microbial species present (Figure S2G). However, monocolonization with *L. reuteri* isolate obtained from the fecal material of this animal failed to induce expansion of CD8αβ$^+$ IELs in the small intestine of IgA-deficient recipients (Figure S2H). Intriguingly, the transfer of fecal material itself was sufficient to drive this response in *Ighasec*$^{-/-}$ hosts (Figure S2H). This suggested that other components of microbiota, not detected by DNA shotgun metagenomic sequencing, are present in the diluted fecal material and induce CD8αβ$^+$ IEL expansion in IgA-deficient hosts. These findings, coupled with the observation that anti-viral gene programs were highly ranked in the gene set enrichment analysis of whole intestinal tissue RNA-seq data for differentially expressed genes between *Ighasec*$^{-/-}$ mice and littermate controls (Figure S2I), led us to investigate the hypothesis that viruses targeted by IgA might be driving the expansion of CD8αβ$^+$ IELs.

To test the hypothesis that viruses were sufficient to drive the CD8αβ$^+$ IEL expansion in IgA-deficient mice, we colonized GF mice with fecal filtrate from *Ighasec*$^{-/-}$ recipient of the diluted fecal material (Figure 3C). Remarkably, the filtrate alone was sufficient to drive the expansion of intraepithelial CD8αβ$^+$ T cells in IgA-deficient recipients (Figure 3D). Furthermore, UV treatment of the filtrate prevented the expansion in *Ighasec*$^{-/-}$ mice, suggesting that CD8αβ$^+$ IEL expansion may require an actively replicating virus (Figure 3D). We next administered an anti-viral drug cocktail consisting of lamivudine, ribavirin, and acyclovir, which targets retroviruses, RNA viruses, and DNA viruses.[28] Strikingly, *Ighasec*$^{-/-}$ mice that had received the anti-viral drug cocktail exhibited a reduction in CD8αβ$^+$ IELs, whereas broad-spectrum antibiotics (ampicillin, vancomycin, metronidazole, and neomycin) had no effect (Figure 3E). The absence of an effect following treatment with the anti-retroviral drugs emtricitabine and tenofovir[29] suggested that viruses other than retroviruses were likely responsible for the expansion of CD8αβ$^+$ IELs.

Since neither eukaryotic DNA viruses detected by metagenomic sequencing (Figure S2G) nor anti-retroviral treatment altered CD8αβ$^+$ IEL expansion (Figure 3E), we hypothesized that RNA virus may be driving the IEL response. Analysis of the intestinal tissue RNA-seq data of the diluted fecal material recipient mice and SPF mice from Barrier II facility (*Hpp*$^-$, SFB$^-$, and MNV$^-$) identified murine astrovirus (MuAstV) as a potential candidate (Figure S2J). MuAstV is a positive-sense, single-stranded RNA virus endemic to many mouse facilities,[30] which can cause chronic infections in RAG-deficient hosts.[31] While MuAstV was present at very low levels in SPF *Ighasec*$^{+/-}$ mice, there was a 1,000-fold increase in viral load across the small intestine of SPF *Ighasec*$^{-/-}$ hosts (Figure 3F). MuAstV was undetectable in GF *Ighasec*$^{+/-}$ or *Ighasec*$^{-/-}$ animals (Figure 3F). Furthermore, taking advantage of the existence of CD8αβ$^+$ low

All data in this figure are represented as mean or mean ± SEM. ****$p < 0.0001$, ***$p < 0.001$, **$p < 0.01$, *$p < 0.05$, ns $p \geq 0.05$. LR mixed effect model (A), false discovery rate (FDR)-adjusted $p < 0.05$; $\log_2$-fold change, $\log_2$fold change (FC) > 0.25 using logistic regression test (D).
(E) UMAP (as in B), with cells colored (blues, *Ighasec*$^{+/-}$ mice; reds, *Ighasec*$^{-/-}$ mice) according to the indicated public TRB CDR3 amino acid motif (top) sharing, and in gray otherwise. Periods in the motif CASS.G represent gaps.

Ighasec$^{-/-}$ litters (Figure 3B), we found that the presence of MuAstV correlated with the expansion of CD8αβ^{+} IELs (Figure 3G).

We next tested whether the presence of MuAstV was sufficient for the CD8αβ^{+} IEL expansion in *Ighasec*$^{-/-}$ mice from Barrier II facility (SFB^{-}, *Hpp*$^{-}$, and MNV^{-}). As shown in Figure 3H, colonization of *Ighasec*$^{-/-}$ GF mice with fecal microbiota from *Ighasec*$^{-/-}$ CD8αβ^{+} low donor, in which MuAstV was undetectable, failed to induce the expansion of CD8αβ^{+} IELs. However, supplementing this microbiota with MuAstV drove the expansion of CD8αβ^{+} IEL in *Ighasec*$^{-/-}$ but not in control mice. Furthermore, monoassociation with MuAstV was sufficient to drive CD8αβ^{+} IEL expansion in *Ighasec*$^{-/-}$ that reached levels comparable to those found in SPF *Ighasec*$^{-/-}$ mice (Figure 3H). Together, these data show that MuAstV but not other members of UofC Barrier II microbiota drive the expansion of CD8αβ^{+} IELs in IgA-deficient animals.

MuAstV was shown to infect goblet cells and enterocytes in the small intestine.[32] Depletion of CD8αβ cells with an anti-CD8β depleting antibody revealed that CD8αβ^{+} IELs play an important role in regulating the MuAstV load in intestinal epithelial cells (IECs) of *Ighasec*$^{-/-}$ mice (Figure 3I). Furthermore, the absence of CD8αβ^{+} T cells (Figure S2K) led to further increased expression of genes involved in innate immune sensing (TLR3 and MyD88), inhibition of viral replication (ZC3HAV1, Adar, Eif2ak, and Slfn9), and IFN-inducible proteins (Ifi27l2, IFITM3, and PML) in the small intestinal tissue of *Ighasec*$^{-/-}$ but not control mice (Figure 3J). Collectively, these data demonstrate that, while unable to clear the virus, CD8αβ^{+} IELs maintain homeostasis by regulating viral load and limiting host innate immune responses.

GC-derived IgA PCs control the colonization of MuAstV in the small intestine

In control *Ighasec*$^{+/-}$ mice, 7 days after MuAstV monoassociation, we noted a significant increase in both the frequency and number of IgA-switched germinal center (GC) B cells in PPs) but not in the mesenteric lymph nodes (mLNs) (Figures 4A and 4B). Additionally, overtime, monoassociation with MuAstV led to the accumulation of IgA PCs in the lamina propria of the small intestine (Figure 4C). This observation, along with the finding that MuAstV colonizes in small intestine in the absence of SIgA (Figure 3F), suggests that SIgA prevents viral colonization by coating the virus. To test this hypothesis, we isolated SIgA from feces of GF or monoassociated *Ighasec*$^{+/-}$ mice using protein L magnetic beads[9] and quantified MuAstV in the IgA-bound versus IgA-unbound fraction. Consistent with our hypothesis, MuAstV was enriched in IgA-bound fraction (Figure 4D). Together, these data indicate that under physiological conditions, MuAstV induces IgA switching in GCs and the generation of lamina propria IgA PCs, which likely control the MuAstV load in the small intestine by coating the virus.

We next assessed the T follicular helper (T_{FH}) response and IgA switching in *Ighasec*$^{-/-}$ mice during chronic MuAstV colonization, as these mice retain the capacity to undergo IgA switching (Figure S1B). As shown in Figures S3A and S3B, MuAstV induced expansion of T_{FH} cells and increased IgA class switching in the PPs 28 days after MuAstV monoassociation. Furthermore, in agreement with these data, MuAstV-colonized SPF *Ighasec*$^{-/-}$ mice displayed PP hyperplasia (Figure S3C), increased cellularity, T_{FH} cells, and IgA switching compared with SPF control mice (Figures S3D–S3F). However, the overall number of PPs remained unchanged (Figure S3G). Taken together, these findings suggest that, although IgA class switching can occur via both T-independent and T-dependent mechanisms,[1,33] MuAstV conspicuously promotes a T-dependent GC IgA response.

T-dependent IgA responses take place in GCs of mLNs and PPs, where B cells can undergo somatic hypermutation and affinity maturation through interaction with T_{FH} cells.[34] To formally test whether T-dependent IgA responses were required to control MuAstV, we analyzed Bcl6$^{fl/fl}$ mice crossed with CD4-Cre or CD21-Cre, lacking T_{FH} or GC B cells, respectively. Noteworthy, these mice exhibited a comparable number of IgA PCs in the small intestinal lamina propria to control animals (Figures S3H and S3I). In accordance with our hypothesis, T_{FH} or GC B cell-deficient mice displayed an expansion of MuAstV in the intestinal tissues (Figures 4E and 4F) that was associated with an expansion of CD8αβ^{+} IELs in the small intestine (Figure 4G), similarly to what was observed in *Ighasec*$^{-/-}$ mice (Figures 1B and 3G).

Overall, these data demonstrate that GC-derived IgA PCs regulate MuAstV load in the small intestine, maintaining immune homeostasis and limiting CD8αβ^{+} T cell expansion.

IgA is essential to prevent small intestinal colonization by select RNA viruses like MNV CR6

We next sought to determine whether IgA's role in limiting viral colonization and CD8αβ^{+} IEL expansion extends to other RNA viruses. To investigate this, we exposed GF *Ighasec*$^{-/-}$ and wild-type animals to enteric viruses belonging to the *Caliciviridae* and *Reoviridae* families and assessed CD8αβ^{+} IEL numbers in the small intestine and tissue viral load. Chronic MNV CR6 (MNV-CR6)[35] persisted in the small intestine of *Ighasec*$^{-/-}$ mice 28 days post-exposure, resulting in a 15-fold increase in MNV CR6 load compared with control mice (Figures 5A and S4A). Furthermore, and in contrast to MNV-CR6, MNV-CW3 (Figure 5A), murine rotavirus (epizootic diarrhea of infant mice [EDIM]) (Figure 5B), and the reovirus T1L strain (Figure 5C) were cleared from the small intestine by day 28 and did not induce small intestinal CD8αβ^{+} IEL expansion (Figure 5D). Notably, MNV-CR6 persistence (Figures 5A and S4A) was associated with an expansion of CD8αβ^{+} IELs in the small intestine (Figures 5D and S4E). Conversely, MNV-CR6 colonized the colon of both *Ighasec*$^{-/-}$ and wild-type mice similarly (Figures S4A and S4B) without inducing CD8αβ^{+} IEL expansion (Figure S4E). These observations suggest IgA restricts enteric viruses beyond MuAstV, such as MNV-CR6, to limit CD8αβ^{+} IEL expansion. However, while SIgA plays a role in preventing reinfection with reovirus[15] and rotavirus,[17] it does not play a role in preventing chronic colonization of the gut by these enteric viruses, indicating a selective role of SIgA in regulating the gut virome.

IgA restricts norovirus colonization to protect the host against immunopathology

Building on our demonstration that IgA is essential for preventing chronic colonization by viruses such as MNV-CR6 and MuAstV, we next investigated whether the expansion of enteric viruses in

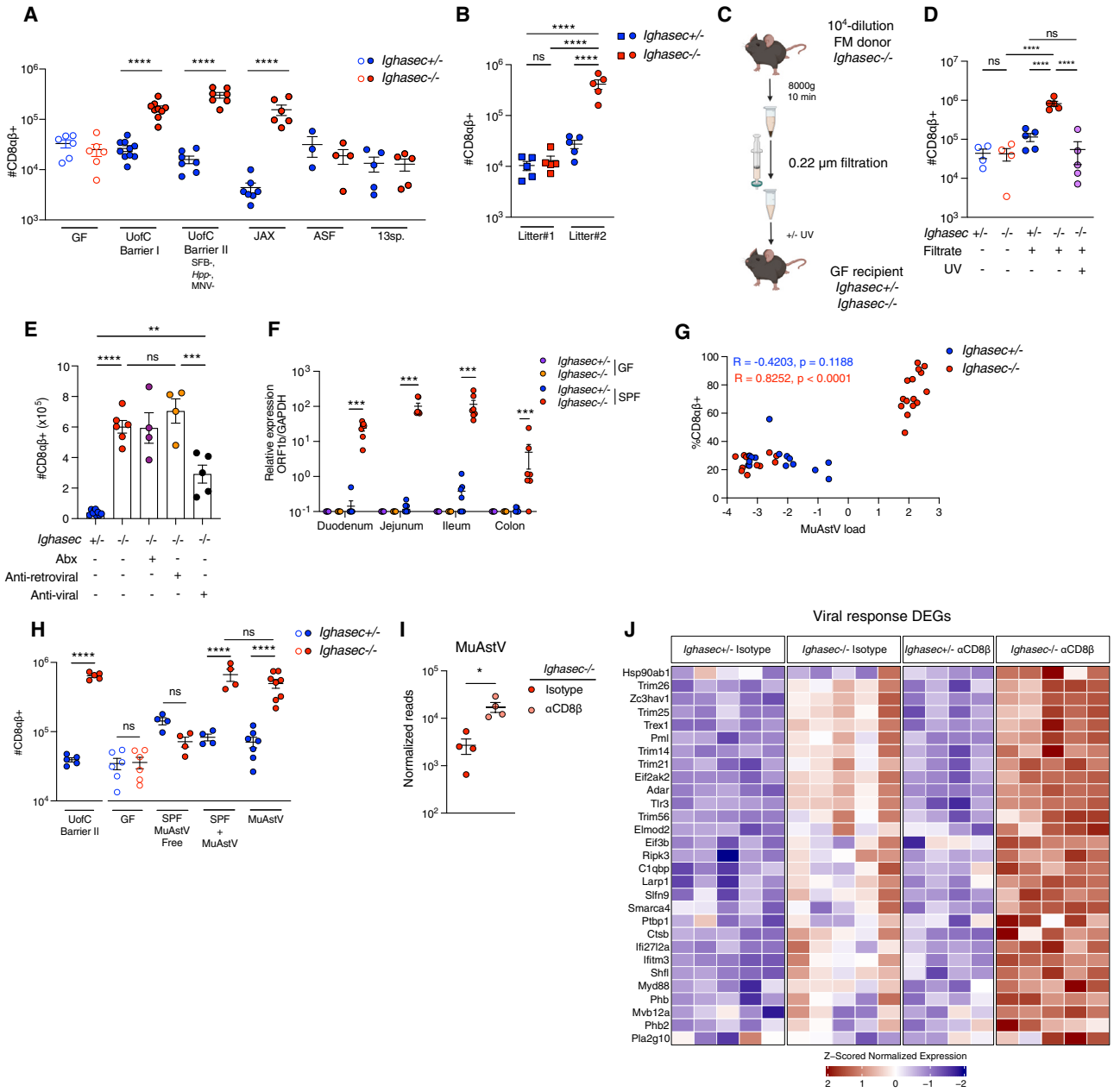

Figure 3. IgA controls MuAstV to limit inflammation in the small intestine

(A) Number of CD8αβ$^+$ IELs in the jejunum of ex-GF *Ighasec*$^{+/-}$ and *Ighasec*$^{-/-}$ mice colonized with different microbiota (x axis). n = 4–9 mice/group.

(B) Number of CD8αβ$^+$ IELs in the jejunum of *Ighasec*$^{+/-}$ and *Ighasec*$^{-/-}$ mice from different litters (x axis). n = 5 mice/group.

(C) Experimental scheme of fecal material filtration and UV inactivation experiment in *Ighasec*$^{+/-}$ and *Ighasec*$^{-/-}$ mice.

(D) Number of CD8αβ$^+$ IELs in the jejunum of GF control or filtrate (with or without UV inactivation) colonized *Ighasec*$^{+/-}$ and *Ighasec*$^{-/-}$ mice. n = 4–5 mice/group.

(E) Number of CD8αβ$^+$ IELs in the jejunum of SPF-, broad-spectrum antibiotic-, anti-retroviral-, and anti-viral-treated *Ighasec*$^{+/-}$ and *Ighasec*$^{-/-}$ mice. n = 4–6 mice/group.

(F) MuAstV load, as measured by qPCR, relative to *Gapdh* in each intestinal segment of GF and SPF *Ighasec*$^{+/-}$ and *Ighasec*$^{-/-}$ mice. n = 7 mice/group.

(G) Paired analysis of CD8αβ$^+$ IEL frequency and MuAstV load in the jejunum of *Ighasec*$^{+/-}$ and *Ighasec*$^{-/-}$ mice. Annotated with Pearson correlation coefficient and p value.

(H) Number of CD8αβ$^+$ IELs in the jejunum of SPF and GF *Ighasec*$^{+/-}$ and *Ighasec*$^{-/-}$, or ex-GF *Ighasec*$^{+/-}$ and *Ighasec*$^{-/-}$ mice 4 weeks after colonization with MuAstV-free microbiota (SPF MuAstV free), MuAstV-free microbiota supplemented with MuAstV (SPF + MuAstV), or MuAstV alone (MuAstV). n = 4–7 mice/group.

(I) Normalized reads of MuAstV in sorted jejunal epithelial cells of isotype and anti-CD8β-treated *Ighasec*$^{-/-}$ mice. n = 4 mice/group.

(J) Heatmap of the Z scored expression of viral response genes (rows) in the ileal tissue of isotype and anti-CD8β-treated *Ighasec*$^{+/-}$ and *Ighasec*$^{-/-}$ mice. n = 5 mice/group.

All data in this figure are pooled from at least two independent experiments and are represented as mean or mean ± SEM. ****$p < 0.0001$, ***$p < 0.001$, **$p < 0.01$, *$p < 0.05$, ns $p \geq 0.05$. Unpaired t test (A and I), ANOVA with Tukey multiple comparison test (B, D, E, and G), Mann-Whitney test (F).

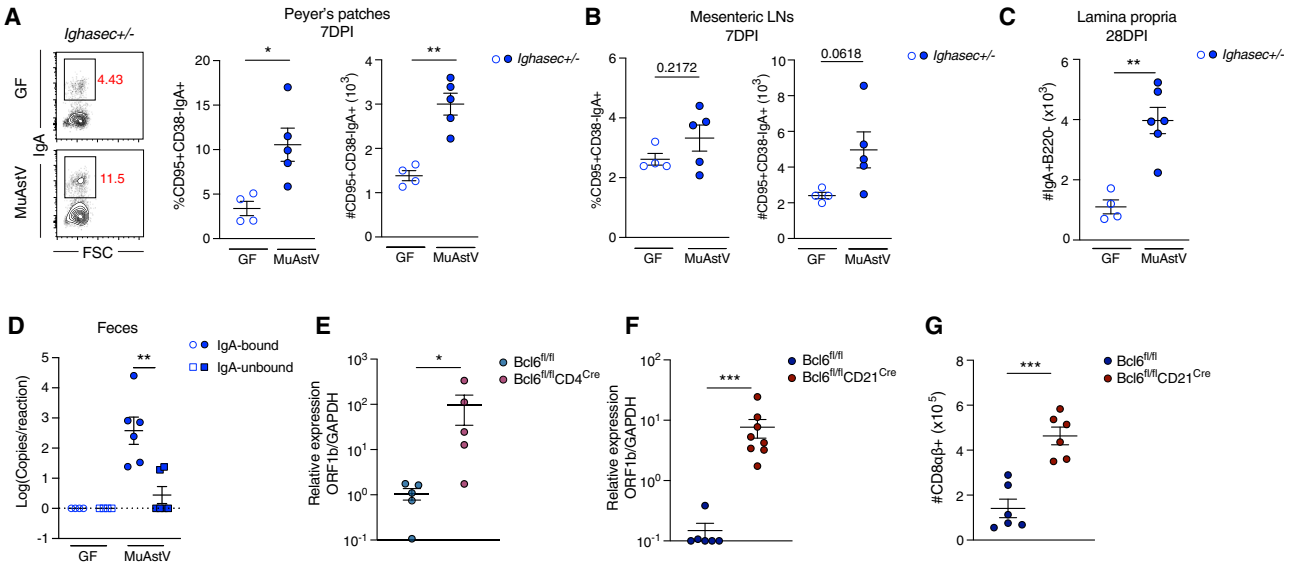

Figure 4. GC-derived IgA PCs contribute to MuAstV control in the small intestine

(A and B) Frequency of IgA-switched cells among $CD38^{-}CD95^{+}$ GC B cells in the PPs (A) and mLNs (B) of GF or MuAstV-monocolonized *Ighasec*$^{+/-}$ mice 7 days after initial inoculation. n = 4–5 mice/group.

(C) Number of IgA^{+} PCs in the jejunal LP of GF or MuAstV-monocolonized *Ighasec*$^{+/-}$ mice. n = 4–6 mice/group.

(D) Number of MuAstV copies per reaction in the fecal extracts of *Ighasec*$^{+/-}$ in IgA-bound and IgA-unbound fractions. n = 4–6 mice/group.

(E and F) MuAstV load, as measured by qPCR, relative to *Gapdh* in the jejunum of $Bcl6^{fl/fl}$ and $Bcl6^{fl/fl}CD4^{Cre}$ (G) or $Bcl6^{fl/fl}$ and $Bcl6^{fl/fl}CD21^{Cre}$ mice (H). n = 5–8 mice/group.

(G) Number of $CD8\alpha\beta^{+}$ IELs in jejunum of SPF $Bcl6^{fl/fl}$ and $Bcl6^{fl/fl}CD21^{Cre}$ mice. n = 6 mice/group.

All data in this figure are pooled from at least two independent experiments and are represented as mean or mean ± SEM. $^{****}p < 0.0001$, $^{***}p < 0.001$, $^{**}p < 0.01$, $^{*}p < 0.05$, ns $p \geq 0.05$. Unpaired t test (A, B, C, and G), Mann-Whitney test (D, E, and F).

IgA-deficient mice influences their susceptibility to immunopathology. We first exposed IgA-deficient mice and controls from the UofC Barrier I (*Hpp*$^{+}$, SFB^{+}, and MNV^{+}) to 2% dextran sulfate sodium (DSS) for 7 days to induce intestinal tissue damage. At baseline, we did not observe any difference in intestinal permeability in the IgA-deficient mice raised in this barrier facility (Figure S5A). However, after DSS administration, we observed significant colonic shortening (Figure S5B) and bacterial translocation to the mLNs (Figure S4C).

We next sought to determine whether the presence of MuAstV or MNV-CR6 in the microbiome impacts colitis outcomes in IgA-deficient animals. Both viruses expanded in tissue of IgA-deficient animals (Figures 3F and S4B) and induced $CD8\alpha\beta^{+}$ IEL response (Figures 3H and 5A). Noteworthy, *Ighasec*$^{-/-}$ mice exhibited 78.5-fold increase in MNV-CR6 fecal shedding 28 days post infection compared with wild-type animals (Figure 6A). This was of particular interest, as MNVs have previously been identified to exacerbate colitis in genetically susceptible hosts.[36] To further investigate, we utilized mice propagated from MuAstV-free litters (Figure 3B) raised in UofC Barrier II, which lack MNVs. We exposed MuAstV- and MNV-free *Ighasec*$^{+/-}$ and *Ighasec*$^{-/-}$ mice from Barrier II (*Hpp*$^{-}$ and SFB^{-}) to MNV-CR6, and 3–4 weeks later subjected them to 2.5% DSS for 7 days to induce colitis. Strikingly, IgA-deficient mice exposed to MNV-CR6 experienced significantly greater weight loss (Figure 6B), colonic shortening (Figure 6C), and colon pathology (Figure 6D) than sham-treated *Ighasec*$^{-/-}$ or MNV-CR6-infected *Ighasec*$^{+/-}$ littermate controls (Figure 6B). Furthermore, no significant difference in weight loss or colonic pathology was observed in *Ighasec*$^{-/-}$ mice colonized with MuAstV (Figures 6B–6D). These results suggest that SIgA is critical to prevent colitis when mice are exposed to MNV-CR6 and exogenous colitogenic trigger but not when colonized with MuAstV.

We next wanted to extend these findings to a genetically susceptible interleukin (IL)-10$^{-/-}$ mouse model of colitis. Previous reports identified elevated luminal IgA levels in IL-10-deficient hosts[37] and increased mucosal inflammation after MNV exposure.[38–40] To determine the role of IgA in the development of colitis in IL-10-deficient mice, we first transferred MNV-positive conventional microbiota from UofC Barrier I (SFB^{+}, Hpp^{+}) to GF *Ighasec*$^{-/-}$IL-10$^{-/-}$ or *Ighasec*$^{+/-}$IL-10$^{-/-}$ hosts. IL-10-deficient hosts lacking IgA lost more body weight than wild-type control mice (Figure S5D) and exhibited more colonic pathology at the experimental endpoint (Figure S5E). To more specifically demonstrate the impact of MNV-CR6 on colitis development in IL-10-deficient mice lacking IgA, we transferred MuAstV-free UofC Barrier II microbiota (SFB^{-}, Hpp^{-}, MNV^{-}) with or without MNV-CR6 to *Ighasec*$^{+/-}$IL-10$^{-/-}$ or *Ighasec*$^{-/-}$IL-10$^{-/-}$ mice. Notably, 89% of the *Ighasec*$^{-/-}$IL-10$^{-/-}$ mice colonized with UofC Barrier II microbiota and MNV-CR6 developed rectal prolapses by the experimental endpoint (Figure 6E) and had increased colonic pathology (Figures 6F and 6G). In sharp contrast, none of the MNV-CR6-infected *Ighasec*$^{+/-}$IL-10$^{-/-}$ hosts and only one *Ighasec*$^{-/-}$IL-10$^{-/-}$ mouse (11%) receiving MNV-free UofC Barrier II microbiota developed rectal prolapse by the experimental endpoint (Figure 6E).

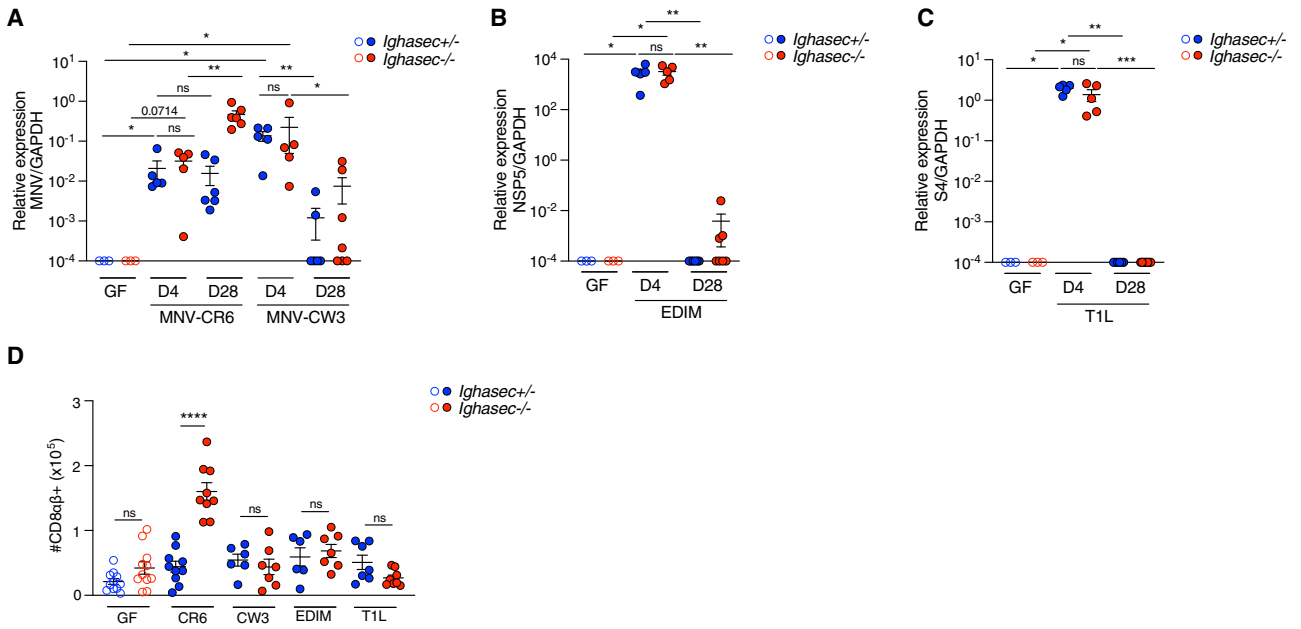

Figure 5. IgA prevents MNV-CR6 expansion in the small intestine

(A–C) MNV-CR6 and MNV-CW3 (A), rotavirus EDIM (B), and reovirus T1L (C) load, as measured by qPCR, relative to *Gapdh* in the jejunum of GF and infected *Ighasec*$^{+/-}$ and *Ighasec*$^{-/-}$ mice at early (day 4) and late (day 28) post-infection time points. n = 3–7 mice/group.

(D) Number of CD8αβ^{+} IELs in the jejunum of ex-GF *Ighasec*$^{+/-}$ and *Ighasec*$^{-/-}$ mice colonized with different viruses (x axis). n = 6–9 mice/group.

All data in this figure are pooled from at least two independent experiments and are represented as mean or mean ± SEM. ****$p < 0.0001$, ***$p < 0.001$, **$p < 0.01$, *$p < 0.05$, ns $p \geq 0.05$. °°°$p < 0.001$, °°$p < 0.01$, °$p < 0.05$. Mann-Whitney test (A–C). Unpaired t test (D).

Overall, these observations suggest that the combination of IgA deficiency and MNV presence heightens susceptibility to colitis but only in genetically susceptible mice or when subjected to a colitogenic trigger.

DISCUSSION

Numerous epidemiological studies suggest a potential role for GC IgA responses in maintaining homeostasis, preventing infections, and mitigating the development of immune-mediated disorders.[3,4,8,17,41–44] However, the rarity of overt disease in patients or mice with IgA deficiency raises questions about the precise role of IgA in pathophysiology and the potential compensatory role of IgM in preventing pathology.

In this study, we found that SIgA responses regulate colonization of the small intestine by MuAstV and MNV-CR6 but not by MNV-CW3, reovirus T1L, or murine rotavirus, which are cleared by other mechanisms, including innate cytokines such as type I IFNs.[45] This finding indicates that SIgA is specifically required to inhibit the colonization of the gut by a select group of RNA viruses and that understanding the development of immunopathology in IgA-deficient patients necessitates studying viruses at the strain level. Whether SIgA controls the colonization of the gut by DNA or other RNA viruses than MuAstV and MNV remains to be determined.

Potential for IgM compensation was confounding the determination of IgA function. Intriguingly, despite the elevated serum IgM and IgM PCs in the intestinal lamina propria, expansion of CD8αβ^{+} IELs and persistent MuAstV infection was also evident in *Igha*$^{-/-}$ hosts. These data suggest that the IgM response may not qualitatively substitute for the IgA responses. This agrees with the recent findings emphasizing that the expression of IgA B cell receptor (BCR) supports efficient B cell participation in PP GCs, memory B cell, and PC generation.[46]

While the absence of IgA has been linked to an increased risk of various immune-mediated disorders, only 20%–30% of individuals with selective IgA deficiency are affected.[3,41] Similarly, our IgA-deficient mouse colonies did not exhibit overt disease symptoms or alterations in intestinal morphology, even when colonized with MuAstV or MNV and showing expansion of CD8αβ^{+} IELs. Moreover, we show that the emergence of immunopathology in the absence of IgA is contingent upon both the specific characteristics of the viral agent and the presence of additional genetic or environmental trigger. Specifically, IgA-deficient mice developed colitis only after exposure to a specific virus such as MNV-CR6 (but not MuAstV, despite IgA being required to control the expansion of both viruses in the small intestine), and the presence of a secondary colitogenic factor, such as IL-10 deficiency or DSS treatment. This dual requirement may explain the relatively rare occurrence of immune-mediated disorders in individuals with selective IgA deficiency.

The role of antigen-driven expansion of proinflammatory CD8αβ^{+} IELs in immunopathology associated with IgA deficiency remains unclear. On one hand, CD8αβ^{+} IELs may protect the host by regulating viral load and preventing the activation of proinflammatory innate immune responses, such as type I IFNs, thereby maintaining tissue homeostasis. On the other hand, the inherently proinflammatory nature of CD8αβ^{+} IELs could impose a fitness cost on the host by increasing susceptibility

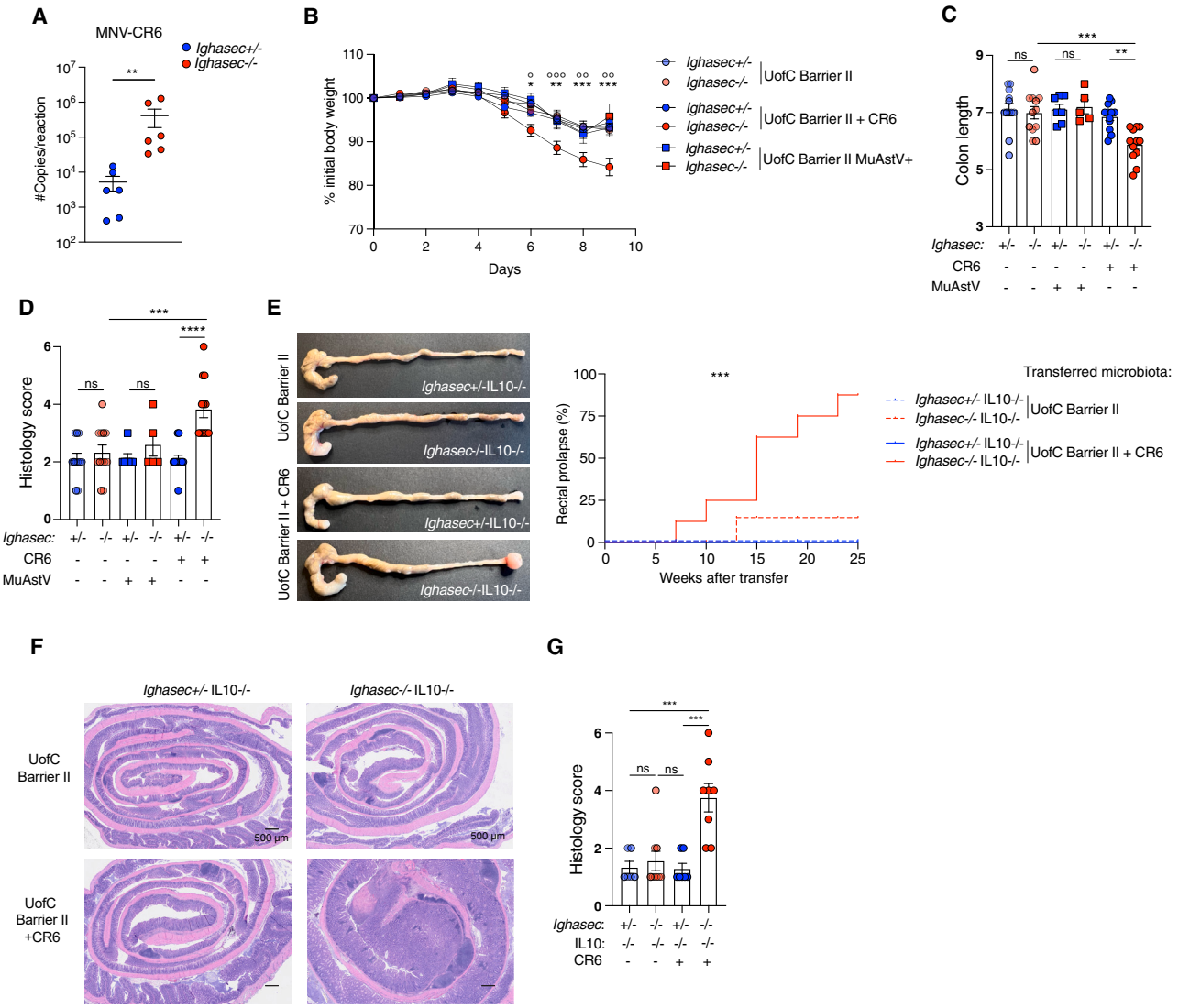

Figure 6. IgA maintains intestinal homeostasis to protect the host from immunopathology

(A) Number of MNV-CR6 copies per reaction in feces of *Ighasec*$^{+/-}$ and *Ighasec*$^{-/-}$ mice 28 days after MNV-CR6 infection. *n* = 6 mice/group.

(B and C) Percent of initial body weight change (B) and colonic shortening (C) of the *Ighasec*$^{+/-}$ or *Ighasec*$^{-/-}$ virus-free or MNV-CR6 infected, and MuAstV^{+} mice after exposure to 2.5% DSS in water. *n* = 5–12 mice/group. In (B), ° indicates the effect due to the infection status (i.e., *Ighasec*$^{-/-}$ UofC Barrier II versus *Ighasec*$^{-/-}$ UofC Barrier II + CR6), while * indicates the effect due to genotype (i.e., *Ighasec*$^{+/-}$ UofC Barrier II + CR6 versus *Ighasec*$^{-/-}$ UofC Barrier II + CR6) at given time points.

(D) Colon tissue Swiss roll histology scores of the *Ighasec*$^{+/-}$ or *Ighasec*$^{-/-}$ virus-free or MNV-CR6 infected, and MuAstV^{+} mice after exposure to 2.5% DSS in water. *n* = 5–12 mice/group.

(E) Representative image (left) and rectal prolapse incidences (right) in *Ighasec*$^{+/-}$ IL-10$^{-/-}$ and *Ighasec*$^{-/-}$IL-10$^{-/-}$ mice colonized with UofC Barrier II virus-free microbiota or UofC Barrier II virus-free microbiota and MNV-CR6. *n* = 6–9 mice/group.

(F) Representative H&E staining of the colon from (E) at the onset of the prolapse.

(G) Colon tissue Swiss roll histology scores of the *Ighasec*$^{+/-}$IL-10$^{-/-}$ and *Ighasec*$^{-/-}$IL-10$^{-/-}$ mice colonized with UofC Barrier II microbiota or UofC Barrier II microbiota with MNV-CR6. *n* = 6–9 mice/group.

All data in this figure are pooled from at least two independent experiments and are represented as mean or mean ± SEM. ****$p < 0.0001$, ***$p < 0.001$, **$p < 0.01$, *$p < 0.05$, ns $p \geq 0.05$. °°°$p < 0.001$, °°$p < 0.01$, °$p < 0.05$. Mann-Whitney test (A), unpaired t test (B), ANOVA with Tukey multiple comparison test (C, D, and G), and Mantel-Cox test (E).

to immunopathological conditions, despite their role in controlling viral load. For instance, this was shown in mice lacking the transcription factor GATA4 in IECs, where alterations in SFB colonization led to dysregulated inflammatory T cell responses that in turn promoted immunopathology.[9] This example highlights the delicate balance between immune regulation and potential immunopathology, suggesting that while CD8αβ^{+} IELs are essential for controlling pathogens, their proinflammatory characteristics could also lead to detrimental effects under specific conditions of IgA deficiency.

The prevalence of gastrointestinal viruses, prolonged viral shedding, and gastrointestinal symptoms is notably higher in common variable immunodeficiency (CVID) patients, particularly those with very low serum and mucosal IgA levels.[47] Chronic norovirus infection in CVID patients was associated with inflammation and enteropathy.[48] These patients also exhibit an increase in type I IFN gene signatures and an increase in the number of IELs in intestinal biopsies.[48,49] While CVID can affect the production of other immunoglobulin isotypes besides IgA, the absence of mucosal IgA PCs specifically was correlated with increased inflammation and disrupted tissue homeostasis.[48] These consequences were further exacerbated in the presence of norovirus infection. Taken together, these observations in humans and our findings in mice highlight an important link between IgA deficiency, failure to regulate chronic colonization by select viral pathobionts, dysregulated inflammatory immune responses, and disease. The place of viruses in IgA-mediated immunopathology relative to other types of microbes, such as commensal or pathogenic bacteria, remains an open question that warrants further exploration.

RESOURCE AVAILABILITY

Lead contact

Further information, requests for resources, and reagents should be directed to and will be fulfilled by the lead contact, Bana Jabri (bjabri@bsd.uchicago.edu).

Materials availability

All reagents generated or used in this study are available on request from the lead contact with a completed Materials Transfer Agreement. Information on reagents used in this study is available in the key resources table.

Data and code availability

Metagenomic and 16S rRNA gene raw sequencing data have been deposited at NCBI Sequence Read Archive and are available under the accession BioProject ID PRJNA1212528. Bulk and single-cell RNA-seq raw data have been deposited and are available in GEO under the accession numbers GEO: GSE289917, GSE289554, and GSE289553.

This paper does not generate original code.

Any additional information required to reanalyze the data reported in this work paper is available from the lead contact upon request.

ACKNOWLEDGMENTS

We thank Ken Caldwell, Christiane Wobus, and Nihal Altan-Bonnet for sharing NYU1 MuAstV, MNV-CR6/CW3, and EDIM, respectively. We thank Betty Theriault, Kristin Kolar, Emma Elmiger, and the entire Gnotobiotic Research Animal Facility at the University of Chicago for their help with the experiments involving gnotobiotic mice. We thank Cezary Ciszewski of the Human Disease and Immune Discovery for his technical support. We thank the Human Tissue Resource Center, the Integrated Light Microscopy Core Facility, and the Genomics Facility at the University of Chicago for their technical support. This study was supported by NIH grants 5R37-AI038339-27 to A.B., R01DK06718-16 to B.J., and Digestive Diseases Research Core Center C-IID P30 DK42086 at the University of Chicago to B.J. and A.B. Z.M.E. was supported by NIAID T32 AI007334 and AR079068 grants. This work is dedicated to A.B., who passed away during manuscript preparation. The graphical abstract was created in BioRender (Lisicka, W. [2025]; https://BioRender.com/o78j530).

AUTHOR CONTRIBUTIONS

A.B. and B.J. conceived the study. A.B., B.J., Z.M.E., and W.L. designed the study and interpreted the data. A.B. and S.A.E. conceived the design of the *Ighasec*$^{-/-}$ mice, and S.A.E. generated the mice. Z.M.E., W.L., and J.R.M. performed the experiments, and W.L. and Z.M.E. analyzed the data. J.J.S. and S.J.R. analyzed and interpreted the scRNA-seq, TCR repertoire, and tissue RNA-seq data. Tissue RNA-seq data analysis helped to formulate the hypothesis implicating viruses in driving CD8$\alpha\beta^{+}$ IEL expansion. N.J.W.-W. performed the 16S rRNA and metagenomic sequencing. N.J.W.-W. and R.F.I. performed the downstream analysis. S.R.K. recovered MuAstV reads from whole-tissue RNA-seq data, and Y.B. provided insight on *in vivo* anti-retroviral treatments. J.G.C. provided the GC B cell and T_{FH} cell-deficient mice and supervised experiments involving these mice. W.L., Z.M.E., and B.J. wrote the manuscript. W.L., Z.M.E., J.J.S., N.J.W.-W., J.G.C., Y.B., and R.F.I. edited the manuscript. R.F.I., J.G.C., B.J., and A.B. acquired the funds to support the work. A.B. and B.J. directed the study. All authors reviewed and approved the final manuscript except A.B., who passed away during manuscript preparation.

DECLARATION OF INTERESTS

The authors declare no competing interests.

STAR★METHODS

Detailed methods are provided in the online version of this paper and include the following:

- KEY RESOURCES TABLE
- EXPERIMENTAL MODELS AND STUDY PARTICIPANT DETAILS
  - Mice
  - Antibiotic and antiviral treatments
  - Viral infections
  - Microbial transfers
  - DSS-induced colitis
- METHOD DETAILS
  - Isolation of intraepithelial and lamina propria lymphocytes
  - Single cell tissue suspensions
  - Ex-vivo cell stimulation
  - Flow cytometry
  - Bacterial flow cytometry
  - In-vivo cell depletion
  - ELISA
  - Histology
  - DNA isolation
  - Microbial 16S rRNA Gene Sequencing
  - Microbial DNA Shotgun Sequencing
  - IgA-MuAstV pulldown
  - RNA isolation
  - qPCR
  - RNA-seq library preparation
  - Single cell RNA-seq
- QUANTIFICATION AND STATISTICAL ANALYSIS
  - Analysis of Microbial 16S rRNA Gene Sequencing and Microbial DNA Shotgun Sequencing
  - Recovery of viral reads from the bulk RNA-seq
  - Mouse bulk RNA-seq data analysis: Quality control filtering and normalization
  - Mouse bulk RNA-seq data analysis: Differential expression and gene set enrichment
  - Mouse bulk RNA-seq data analysis: Visualization
  - Mouse single cell RNA-seq data analysis: Quality control and normalization
  - Mouse single cell RNA-seq data analysis: Clustering and identification of functional cluster markers
  - Mouse single cell RNA-seq data analysis: Identifying expanded clones and enriched motifs
  - Mouse single cell RNA-seq data analysis: Visualization

SUPPLEMENTAL INFORMATION

Supplemental information can be found online at https://doi.org/10.1016/j.chom.2025.03.004.

Received: April 23, 2024
Revised: November 26, 2024
Accepted: March 5, 2025
Published: March 27, 2025

REFERENCES

1. Bunker, J.J., Flynn, T.M., Koval, J.C., Shaw, D.G., Meisel, M., McDonald, B.D., Ishizuka, I.E., Dent, A.L., Wilson, P.C., Jabri, B., et al. (2015). Innate and Adaptive Humoral Responses Coat Distinct Commensal Bacteria with Immunoglobulin A. Immunity *43*, 541–553. https://doi.org/10.1016/j.immuni.2015.08.007.
2. van der Heijden, P.J., Stok, W., and Bianchi, A.T. (1987). Contribution of immunoglobulin-secreting cells in the murine small intestine to the total 'background' immunoglobulin production. Immunology *62*, 551–555.
3. Singh, K., Chang, C., and Gershwin, M.E. (2014). IgA deficiency and autoimmunity. Autoimmun. Rev. *13*, 163–177. https://doi.org/10.1016/j.autrev.2013.10.005.
4. Koskinen, S. (1996). Long-term follow-up of health in blood donors with primary selective IgA deficiency. J. Clin. Immunol. *16*, 165–170. https://doi.org/10.1007/BF01540915.
5. Aghamohammadi, A., Cheraghi, T., Gharagozlou, M., Movahedi, M., Rezaei, N., Yeganeh, M., Parvaneh, N., Abolhassani, H., Pourpak, Z., and Moin, M. (2009). IgA deficiency: correlation between clinical and immunological phenotypes. J. Clin. Immunol. *29*, 130–136. https://doi.org/10.1007/s10875-008-9229-9.
6. Ballow, M. (2002). Primary immunodeficiency disorders: antibody deficiency. J. Allergy Clin. Immunol. *109*, 581–591. https://doi.org/10.1067/mai.2002.122466.
7. Collin, P., Mäki, M., Keyriläinen, O., Hällström, O., Reunala, T., and Pasternack, A. (1992). Selective IgA deficiency and coeliac disease. Scand. J. Gastroenterol. *27*, 367–371. https://doi.org/10.3109/00365529209000089.
8. Suzuki, K., Meek, B., Doi, Y., Muramatsu, M., Chiba, T., Honjo, T., and Fagarasan, S. (2004). Aberrant expansion of segmented filamentous bacteria in IgA-deficient gut. Proc. Natl. Acad. Sci. USA *101*, 1981–1986. https://doi.org/10.1073/pnas.0307317101.
9. Earley, Z.M., Lisicka, W., Sifakis, J.J., Aguirre-Gamboa, R., Kowalczyk, A., Barlow, J.T., Shaw, D.G., Discepolo, V., Tan, I.L., Gona, S., et al. (2023). GATA4 controls regionalization of tissue immunity and commensal-driven immunopathology. Immunity *56*, 43–57.e10. https://doi.org/10.1016/j.immuni.2022.12.009.
10. Donaldson, G.P., Ladinsky, M.S., Yu, K.B., Sanders, J.G., Yoo, B.B., Chou, W.C., Conner, M.E., Earl, A.M., Knight, R., Bjorkman, P.J., et al. (2018). Gut microbiota utilize immunoglobulin A for mucosal colonization. Science *360*, 795–800. https://doi.org/10.1126/science.aaq0926.
11. Peterson, D.A., McNulty, N.P., Guruge, J.L., and Gordon, J.I. (2007). IgA response to symbiotic bacteria as a mediator of gut homeostasis. Cell Host Microbe *2*, 328–339. https://doi.org/10.1016/j.chom.2007.09.013.
12. Peterson, D.A., Planer, J.D., Guruge, J.L., Xue, L., Downey-Virgin, W., Goodman, A.L., Seedorf, H., and Gordon, J.I. (2015). Characterizing the interactions between a naturally primed immunoglobulin A and its conserved Bacteroides thetaiotaomicron species-specific epitope in gnotobiotic mice. J. Biol. Chem. *290*, 12630–12649. https://doi.org/10.1074/jbc.M114.633800.
13. Rollenske, T., Burkhalter, S., Muerner, L., von Gunten, S., Lukasiewicz, J., Wardemann, H., and Macpherson, A.J. (2021). Parallelism of intestinal secretory IgA shapes functional microbial fitness. Nature *598*, 657–661. https://doi.org/10.1038/s41586-021-03973-7.
14. Phalipon, A., Kaufmann, M., Michetti, P., Cavaillon, J.M., Huerre, M., Sansonetti, P., and Kraehenbuhl, J.P. (1995). Monoclonal immunoglobulin A antibody directed against sero specific epitope of Shigella flexneri lipopolysaccharide protects against murine experimental shigellosis. J. Exp. Med. *182*, 769–778. https://doi.org/10.1084/jem.182.3.769.
15. Hutchings, A.B., Helander, A., Silvey, K.J., Chandran, K., Lucas, W.T., Nibert, M.L., and Neutra, M.R. (2004). Secretory immunoglobulin A antibodies against the sigma1 outer capsid protein of reovirus type 1 Lang prevent infection of mouse Peyer's patches. J. Virol. *78*, 947–957. https://doi.org/10.1128/jvi.78.2.947-957.2004.
16. Moor, K., Diard, M., Sellin, M.E., Felmy, B., Wotzka, S.Y., Toska, A., Bakkeren, E., Arnoldini, M., Bansept, F., Co, A.D., et al. (2017). High-avidity IgA protects the intestine by enchaining growing bacteria. Nature *544*, 498–502. https://doi.org/10.1038/nature22058.
17. Blutt, S.E., Miller, A.D., Salmon, S.L., Metzger, D.W., and Conner, M.E. (2012). IgA is important for clearance and critical for protection from rotavirus infection. Mucosal Immunol. *5*, 712–719. https://doi.org/10.1038/mi.2012.51.
18. Lycke, N., Erlandsson, L., Ekman, L., Schön, K., and Leanderson, T. (1999). Lack of J chain inhibits the transport of gut IgA and abrogates the development of intestinal antitoxic protection. J. Immunol. *163*, 913–919. https://doi.org/10.4049/jimmunol.163.2.913.
19. Fernandez, M.I., Pedron, T., Tournebize, R., Olivo-Marin, J.C., Sansonetti, P.J., and Phalipon, A. (2003). Anti-inflammatory role for intracellular dimeric immunoglobulin a by neutralization of lipopolysaccharide in epithelial cells. Immunity *18*, 739–749. https://doi.org/10.1016/s1074-7613(03)00122-5.
20. Catanzaro, J.R., Strauss, J.D., Bielecka, A., Porto, A.F., Lobo, F.M., Urban, A., Schofield, W.B., and Palm, N.W. (2019). IgA-deficient humans exhibit gut microbiota dysbiosis despite secretion of compensatory IgM. Sci. Rep. *9*, 13574. https://doi.org/10.1038/s41598-019-49923-2.
21. Barros, M.D., Porto, M.H., Leser, P.G., Grumach, A.S., and Carneiro-Sampaio, M.M. (1985). Study of colostrum of a patient with selective IgA deficiency. Allergol. Immunopathol. (Madr) *13*, 331–334.
22. Fadlallah, J., El Kafsi, H., Sterlin, D., Juste, C., Parizot, C., Dorgham, K., Autaa, G., Gouas, D., Almeida, M., Lepage, P., et al. (2018). Microbial ecology perturbation in human IgA deficiency. Sci. Transl. Med. *10*, eaan1217. https://doi.org/10.1126/scitranslmed.aan1217.
23. Harriman, G.R., Bogue, M., Rogers, P., Finegold, M., Pacheco, S., Bradley, A., Zhang, Y., and Mbawuike, I.N. (1999). Targeted deletion of the IgA constant region in mice leads to IgA deficiency with alterations in expression of other Ig isotypes. J. Immunol. *162*, 2521–2529. https://doi.org/10.4049/jimmunol.162.5.2521.
24. Bonaud, A., Gargowitsch, L., Gilbert, S.M., Rajan, E., Canales-Herrerias, P., Stockholm, D., Rahman, N.F., Collins, M.O., Taskiran, H., Hill, D.L., et al. (2023). Sec22b is a critical and nonredundant regulator of plasma cell maintenance. Proc. Natl. Acad. Sci. USA *120*, e2213056120. https://doi.org/10.1073/pnas.2213056120.
25. Hildner, K., Edelson, B.T., Purtha, W.E., Diamond, M., Matsushita, H., Kohyama, M., Calderon, B., Schraml, B.U., Unanue, E.R., Diamond, M.S., et al. (2008). Batf3 deficiency reveals a critical role for CD8alpha+ dendritic cells in cytotoxic T cell immunity. Science *322*, 1097–1100. https://doi.org/10.1126/science.1164206.
26. Naik, S., Bouladoux, N., Linehan, J.L., Han, S.J., Harrison, O.J., Wilhelm, C., Conlan, S., Himmelfarb, S., Byrd, A.L., Deming, C., et al. (2015). Commensal-dendritic-cell interaction specifies a unique protective skin immune signature. Nature *520*, 104–108. https://doi.org/10.1038/nature14052.
27. Rodgers, J.R., and Cook, R.G. (2005). MHC class Ib molecules bridge innate and acquired immunity. Nat. Rev. Immunol. *5*, 459–471. https://doi.org/10.1038/nri1635.
28. Liu, L., Gong, T., Tao, W., Lin, B., Li, C., Zheng, X., Zhu, S., Jiang, W., and Zhou, R. (2019). Commensal viruses maintain intestinal intraepithelial lymphocytes via noncanonical RIG-I signaling. Nat. Immunol. *20*, 1681–1691. https://doi.org/10.1038/s41590-019-0513-z.
29. Lima-Junior, D.S., Krishnamurthy, S.R., Bouladoux, N., Collins, N., Han, S.J., Chen, E.Y., Constantinides, M.G., Link, V.M., Lim, A.I., Enamorado, M., et al. (2021). Endogenous retroviruses promote homeostatic and inflammatory responses to the microbiota. Cell *184*, 3794–3811.e19. https://doi.org/10.1016/j.cell.2021.05.020.

30. Ng, T.F.F., Kondov, N.O., Hayashimoto, N., Uchida, R., Cha, Y., Beyer, A.I., Wong, W., Pesavento, P.A., Suemizu, H., Muench, M.O., et al. (2013). Identification of an astrovirus commonly infecting laboratory mice in the US and Japan. PLoS One *8*, e66937. https://doi.org/10.1371/journal.pone.0066937.

31. Yokoyama, C.C., Loh, J., Zhao, G., Stappenbeck, T.S., Wang, D., Huang, H.V., Virgin, H.W., and Thackray, L.B. (2012). Adaptive immunity restricts replication of novel murine astroviruses. J. Virol. *86*, 12262–12270. https://doi.org/10.1128/JVI.02018-12.

32. Ingle, H., Hassan, E., Gawron, J., Mihi, B., Li, Y., Kennedy, E.A., Kalugotla, G., Makimaa, H., Lee, S., Desai, P., et al. (2021). Murine astrovirus tropism for goblet cells and enterocytes facilitates an IFN-lambda response in vivo and in enteroid cultures. Mucosal Immunol. *14*, 751–761. https://doi.org/10.1038/s41385-021-00387-6.

33. Macpherson, A.J., Gatto, D., Sainsbury, E., Harriman, G.R., Hengartner, H., and Zinkernagel, R.M. (2000). A primitive T cell-independent mechanism of intestinal mucosal IgA responses to commensal bacteria. Science *288*, 2222–2226. https://doi.org/10.1126/science.288.5474.2222.

34. Mesin, L., Ersching, J., and Victora, G.D. (2016). Germinal Center B Cell Dynamics. Immunity *45*, 471–482. https://doi.org/10.1016/j.immuni.2016.09.001.

35. Nice, T.J., Strong, D.W., McCune, B.T., Pohl, C.S., and Virgin, H.W. (2013). A single-amino-acid change in murine norovirus NS1/2 is sufficient for colonic tropism and persistence. J. Virol. *87*, 327–334. https://doi.org/10.1128/JVI.01864-12.

36. Cadwell, K., Patel, K.K., Maloney, N.S., Liu, T.C., Ng, A.C.Y., Storer, C.E., Head, R.D., Xavier, R., Stappenbeck, T.S., and Virgin, H.W. (2010). Virus-plus-susceptibility gene interaction determines Crohn's disease gene Atg16L1 phenotypes in intestine. Cell *141*, 1135–1145. https://doi.org/10.1016/j.cell.2010.05.009.

37. Gomes-Santos, A.C., Moreira, T.G., Castro-Junior, A.B., Horta, B.C., Lemos, L., Cruz, D.N., Guimarães, M.A.F., Cara, D.C., McCafferty, D.M., and Faria, A.M.C. (2012). New insights into the immunological changes in IL-10-deficient mice during the course of spontaneous inflammation in the gut mucosa. Clin. Dev. Immunol. *2012*, 560817. https://doi.org/10.1155/2012/560817.

38. Basic, M., Keubler, L.M., Buettner, M., Achard, M., Breves, G., Schröder, B., Smoczek, A., Jörns, A., Wedekind, D., Zschemisch, N.H., et al. (2014). Norovirus triggered microbiota-driven mucosal inflammation in interleukin 10-deficient mice. Inflamm. Bowel Dis. *20*, 431–443. https://doi.org/10.1097/01.MIB.0000441346.86827.ed.

39. Lencioni, K.C., Seamons, A., Treuting, P.M., Maggio-Price, L., and Brabb, T. (2008). Murine norovirus: an intercurrent variable in a mouse model of bacteria-induced inflammatory bowel disease. Comp. Med. *58*, 522–533.

40. Bolsega, S., Basic, M., Smoczek, A., Buettner, M., Eberl, C., Ahrens, D., Odum, K.A., Stecher, B., and Bleich, A. (2019). Composition of the Intestinal Microbiota Determines the Outcome of Virus-Triggered Colitis in Mice. Front. Immunol. *10*, 1708. https://doi.org/10.3389/fimmu.2019.01708.

41. Rawla, P., Killeen, R.B., and Joseph, N.I. (2024). Selective IgA Deficiency. In StatPearls (StatPearls Publishing).

42. Kumar, V., Jarzabek-Chorzelska, M., Sulej, J., Karnewska, K., Farrell, T., and Jablonska, S. (2002). Celiac disease and immunoglobulin a deficiency: how effective are the serological methods of diagnosis? Clin. Diagn. Lab. Immunol. *9*, 1295–1300. https://doi.org/10.1128/cdli.9.6.1295-1300.2002.

43. Mazanec, M.B., Coudret, C.L., and Fletcher, D.R. (1995). Intracellular neutralization of influenza virus by immunoglobulin A anti-hemagglutinin monoclonal antibodies. J. Virol. *69*, 1339–1343. https://doi.org/10.1128/JVI.69.2.1339-1343.1995.

44. French, M.A.H., Denis, K.A., Dawkins, R., and Peter, J.B. (2008). Severity of infections in IgA deficiency: correlation with decreased serum antibodies to pneumococcal polysaccharides and decreased serum IgG2 and/or IgG4. Clin. Exp. Immunol. *100*, 47–53. https://doi.org/10.1111/j.1365-2249.1995.tb03602.x.

45. Johansson, C., Wetzel, J.D., He, J., Mikacenic, C., Dermody, T.S., and Kelsall, B.L. (2007). Type I interferons produced by hematopoietic cells protect mice against lethal infection by mammalian reovirus. J. Exp. Med. *204*, 1349–1358. https://doi.org/10.1084/jem.20061587.

46. Raso, F., Liu, S., Simpson, M.J., Barton, G.M., Mayer, C.T., Acharya, M., Muppidi, J.R., Marshak-Rothstein, A., and Reboldi, A. (2023). Antigen receptor signaling and cell death resistance controls intestinal humoral response zonation. Immunity *56*, 2373–2387.e8. https://doi.org/10.1016/j.immuni.2023.08.018.

47. van de Ven, A.A., Janssen, W.J., Schulz, L.S., van Loon, A.M., Voorkamp, K., Sanders, E.A., Kusters, J.G., Nierkens, S., Boes, M., Wensing, A.M., et al. (2014). Increased prevalence of gastrointestinal viruses and diminished secretory immunoglobulin a levels in antibody deficiencies. J. Clin. Immunol. *34*, 962–970. https://doi.org/10.1007/s10875-014-0087-3.

48. Strohmeier, V., Andrieux, G., Unger, S., Pascual-Reguant, A., Klocperk, A., Seidl, M., Marques, O.C., Eckert, M., Gräwe, K., Shabani, M., et al. (2023). Interferon-Driven Immune Dysregulation in Common Variable Immunodeficiency-Associated Villous Atrophy and Norovirus Infection. J. Clin. Immunol. *43*, 371–390. https://doi.org/10.1007/s10875-022-01379-2.

49. Shulzhenko, N., Dong, X., Vyshenska, D., Greer, R.L., Gurung, M., Vasquez-Perez, S., Peremyslova, E., Sosnovtsev, S., Quezado, M., Yao, M., et al. (2018). CVID enteropathy is characterized by exceeding low mucosal IgA levels and interferon-driven inflammation possibly related to the presence of a pathobiont. Clin. Immunol. *197*, 139–153. https://doi.org/10.1016/j.clim.2018.09.008.

50. Abadie, V., Kim, S.M., Lejeune, T., Palanski, B.A., Ernest, J.D., Tastet, O., Voisine, J., Discepolo, V., Marietta, E.V., Hawash, M.B.F., et al. (2020). IL-15, gluten and HLA-DQ8 drive tissue destruction in coeliac disease. Nature *578*, 600–604. https://doi.org/10.1038/s41586-020-2003-8.

51. Bouziat, R., Biering, S.B., Kouame, E., Sangani, K.A., Kang, S., Ernest, J.D., Varma, M., Brown, J.J., Urbanek, K., Dermody, T.S., et al. (2018). Murine Norovirus Infection Induces T(H)1 Inflammatory Responses to Dietary Antigens. Cell Host Microbe *24*, 677–688.e5. https://doi.org/10.1016/j.chom.2018.10.004.

52. Hou, G., Zeng, Q., Matthijnssens, J., Greenberg, H.B., and Ding, S. (2021). Rotavirus NSP1 Contributes to Intestinal Viral Replication, Pathogenesis, and Transmission. mBio *12*, e0320821. https://doi.org/10.1128/mBio.03208-21.

53. Blanchet, E., Van de Velde, S., Matsumura, S., Hao, E., LeLay, J., Kaestner, K., and Montminy, M. (2015). Feedback inhibition of CREB signaling promotes beta cell dysfunction in insulin resistance. Cell Rep. *10*, 1149–1157. https://doi.org/10.1016/j.celrep.2015.01.046.

54. Burggraf, S., Huber, H., and Stetter, K.O. (1997). Reclassification of the crenarchael orders and families in accordance with 16S rRNA sequence data. Int. J. Syst. Bacteriol. *47*, 657–660. https://doi.org/10.1099/00207713-47-3-657.

55. Caporaso, J.G., Lauber, C.L., Walters, W.A., Berg-Lyons, D., Lozupone, C.A., Turnbaugh, P.J., Fierer, N., and Knight, R. (2011). Global patterns of 16S rRNA diversity at a depth of millions of sequences per sample. Proc. Natl. Acad. Sci. USA *108*, 4516–4522. https://doi.org/10.1073/pnas.1000080107.

56. Bolyen, E., Rideout, J.R., Dillon, M.R., Bokulich, N.A., Abnet, C.C., Al-Ghalith, G.A., Alexander, H., Alm, E.J., Arumugam, M., Asnicar, F., et al. (2019). Reproducible, interactive, scalable and extensible microbiome data science using QIIME 2. Nat. Biotechnol. *37*, 852–857. https://doi.org/10.1038/s41587-019-0209-9.

57. Quast, C., Pruesse, E., Yilmaz, P., Gerken, J., Schweer, T., Yarza, P., Peplies, J., and Glöckner, F.O. (2013). The SILVA ribosomal RNA gene database project: improved data processing and web-based tools. Nucleic Acids Res. *41*, D590–D596. https://doi.org/10.1093/nar/gks1219.

58. Virtanen, P., Gommers, R., Oliphant, T.E., Haberland, M., Reddy, T., Cournapeau, D., Burovski, E., Peterson, P., Weckesser, W., Bright, J., et al. (2020). SciPy 1.0: fundamental algorithms for scientific computing

in Python. Nat. Methods *17*, 261–272. https://doi.org/10.1038/s41592-019-0686-2.

59. Seabold, S.P., and Perktold, J. (2010). statsmodels: Econometric and statistical modeling with python. In Proceedings of the 9th Python in Science Conference, pp. 92–96. https://doi.org/10.25080/Majora-92bf1922-011.
60. Blanco-Míguez, A., Beghini, F., Cumbo, F., McIver, L.J., Thompson, K.N., Zolfo, M., Manghi, P., Dubois, L., Huang, K.D., Thomas, A.M., et al. (2023). Extending and improving metagenomic taxonomic profiling with uncharacterized species using MetaPhlAn 4. Nat. Biotechnol. *41*, 1633–1644. https://doi.org/10.1038/s41587-023-01688-w.
61. Bankhead, P., Loughrey, M.B., Fernández, J.A., Dombrowski, Y., McArt, D.G., Dunne, P.D., McQuaid, S., Gray, R.T., Murray, L.J., Coleman, H.G., et al. (2017). QuPath: Open source software for digital pathology image analysis. Sci. Rep. *7*, 16878. https://doi.org/10.1038/s41598-017-17204-5.
62. Koller, B.H., Marrack, P., Kappler, J.W., and Smithies, O. (2010). Normal development of mice deficient in beta 2M, MHC class I proteins, and CD8+ T cells. 1990. J. Immunol. *184*, 4592–4595.
63. Vugmeyster, Y., Glas, R., Pérarnau, B., Lemonnier, F.A., Eisen, H., and Ploegh, H. (1998). Major histocompatibility complex (MHC) class I KbDb -/- deficient mice possess functional CD8+ T cells and natural killer cells. Proc. Natl. Acad. Sci. USA *95*, 12492–12497. https://doi.org/10.1073/pnas.95.21.12492.
64. Kühn, R., Löhler, J., Rennick, D., Rajewsky, K., and Müller, W. (1993). Interleukin-10-deficient mice develop chronic enterocolitis. Cell *75*, 263–274. https://doi.org/10.1016/0092-8674(93)80068-p.
65. Hall, J.A., Bouladoux, N., Sun, C.M., Wohlfert, E.A., Blank, R.B., Zhu, Q., Grigg, M.E., Berzofsky, J.A., and Belkaid, Y. (2008). Commensal DNA limits regulatory T cell conversion and is a natural adjuvant of intestinal immune responses. Immunity *29*, 637–649. https://doi.org/10.1016/j.immuni.2008.08.009.
66. Ghosh, S., Kumar, M., Santiana, M., Mishra, A., Zhang, M., Labayo, H., Chibly, A.M., Nakamura, H., Tanaka, T., Henderson, W., et al. (2022). Enteric viruses replicate in salivary glands and infect through saliva. Nature *607*, 345–350. https://doi.org/10.1038/s41586-022-04895-8.
67. Dallari, S., Heaney, T., Rosas-Villegas, A., Neil, J.A., Wong, S.Y., Brown, J.J., Urbanek, K., Herrmann, C., Depledge, D.P., Dermody, T.S., et al. (2021). Enteric viruses evoke broad host immune responses resembling those elicited by the bacterial microbiome. Cell Host Microbe *29*, 1014–1029.e8. https://doi.org/10.1016/j.chom.2021.03.015.
68. Bouziat, R., Hinterleitner, R., Brown, J.J., Stencel-Baerenwald, J.E., Ikizler, M., Mayassi, T., Meisel, M., Kim, S.M., Discepolo, V., Pruijssers, A.J., et al. (2017). Reovirus infection triggers inflammatory responses to dietary antigens and development of celiac disease. Science *356*, 44–50. https://doi.org/10.1126/science.aah5298.
69. Janowski, A.B., Bauer, I.K., Holtz, L.R., and Wang, D. (2017). Propagation of Astrovirus VA1, a Neurotropic Human Astrovirus, in Cell Culture. J. Virol. *91*, e00740-17. https://doi.org/10.1128/JVI.00740-17.
70. Lefrançois, L., and Lycke, N. (2001). Isolation of mouse small intestinal intraepithelial lymphocytes, Peyer's patch, and lamina propria cells. Curr. Protoc. Immunol. *Chapter 3*, Unit 3.19. https://doi.org/10.1002/0471142735.im0319s17.
71. Barlow, J.T., Bogatyrev, S.R., and Ismagilov, R.F. (2020). A quantitative sequencing framework for absolute abundance measurements of mucosal and lumenal microbial communities. Nat. Commun. *11*, 2590. https://doi.org/10.1038/s41467-020-16224-6.
72. Bogatyrev, S.R., Rolando, J.C., and Ismagilov, R.F. (2020). Self-reinoculation with fecal flora changes microbiota density and composition leading to an altered bile-acid profile in the mouse small intestine. Microbiome *8*, 19. https://doi.org/10.1186/s40168-020-0785-4.
73. Li, D., Liu, C.M., Luo, R., Sadakane, K., and Lam, T.W. (2015). MEGAHIT: an ultra-fast single-node solution for large and complex metagenomics assembly via succinct de Bruijn graph. Bioinformatics *31*, 1674–1676. https://doi.org/10.1093/bioinformatics/btv033.
74. Buchfink, B., Xie, C., and Huson, D.H. (2015). Fast and sensitive protein alignment using DIAMOND. Nat. Methods *12*, 59–60. https://doi.org/10.1038/nmeth.3176.
75. Dobin, A., Davis, C.A., Schlesinger, F., Drenkow, J., Zaleski, C., Jha, S., Batut, P., Chaisson, M., and Gingeras, T.R. (2013). STAR: ultrafast universal RNA-seq aligner. Bioinformatics *29*, 15–21. https://doi.org/10.1093/bioinformatics/bts635.
76. Love, M.I., Huber, W., and Anders, S. (2014). Moderated estimation of fold change and dispersion for RNA-seq data with DESeq2. Genome Biol. *15*, 550. https://doi.org/10.1186/s13059-014-0550-8.
77. Ritchie, M.E., Phipson, B., Wu, D., Hu, Y., Law, C.W., Shi, W., and Smyth, G.K. (2015). limma powers differential expression analyses for RNA-sequencing and microarray studies. Nucleic Acids Res. *43*, e47. https://doi.org/10.1093/nar/gkv007.
78. Korotkevich, G., Sukhov, V., Budin, N., Shpak, B., Artyomov, M.N., and Sergushichev, A. (2021). Fast gene set enrichment analysis. Preprint at bioRxiv. https://doi.org/10.1101/060012.
79. Gene Ontology Consortium (2021). The Gene Ontology resource: enriching a GOld mine. Nucleic Acids Res. *49*, D325–D334. https://doi.org/10.1093/nar/gkaa1113.
80. Ashburner, M., Ball, C.A., Blake, J.A., Botstein, D., Butler, H., Cherry, J.M., Davis, A.P., Dolinski, K., Dwight, S.S., Eppig, J.T., et al. (2000). Gene ontology: tool for the unification of biology. The Gene Ontology Consortium. Nat. Genet. *25*, 25–29. https://doi.org/10.1038/75556.
81. Gu, Z., Eils, R., and Schlesner, M. (2016). Complex heatmaps reveal patterns and correlations in multidimensional genomic data. Bioinformatics *32*, 2847–2849. https://doi.org/10.1093/bioinformatics/btw313.
82. Hao, Y., Hao, S., Andersen-Nissen, E., Mauck, W.M., 3rd, Zheng, S., Butler, A., Lee, M.J., Wilk, A.J., Darby, C., Zager, M., et al. (2021). Integrated analysis of multimodal single-cell data. Cell *184*, 3573–3587.e29. https://doi.org/10.1016/j.cell.2021.04.048.
83. Hafemeister, C., and Satija, R. (2019). Normalization and variance stabilization of single-cell RNA-seq data using regularized negative binomial regression. Genome Biol. *20*, 296. https://doi.org/10.1186/s13059-019-1874-1.

STAR★METHODS

KEY RESOURCES TABLE

REAGENT or RESOURCE	SOURCE	IDENTIFIER
Antibodies		
CD45 BV421 (30-F11)	Biolegend	Cat#103134; RRID:AB_2562559
CD45 AF532 (30-F11)	Thermo Fisher Scientific	Cat#58-0451-82; RRID:AB_11218871
CD3ε BUV737 (145-2C11)	BD Biosciences	Cat#612771; RRID:AB_2870100
TCRgd FITC (eBioGL3)	Thermo Fisher Scientific	Cat#11-5711-82; RRID:AB_465238
TCRβ BUV737 (H57-597)	BD Biosciences	Cat#612821; RRID:AB_2870145
CD4 BV785 (GK1.5)	Biolegend	Cat#100453; RRID:AB_2565843
CD4 BUV615 (GK1.5)	BD Biosciences	Cat#613006; RRID:AB_2870274
CD4 BUV615 (RM4-4)	BD Biosciences	Cat#751366; RRID:AB_2875373
CD8β BV480 (H35-17.2)	BD Biosciences	Cat#746835; RRID:AB_2744086
CD8β BUV395 (H35-17.2)	BD Biosciences	Cat#740278; RRID:AB_2740017
CD8β AF647 (YTS156.7.7)	Biolegend	Cat#126612; RRID:AB_2075777
CD8α APC/Fire 750 (53-6.7)	Biolegend	Cat#100766; RRID:AB_2572113
CD8α APC-Cy7 (53-6.7)	Biolegend	Cat#100714; RRID:AB_312753
CD103 BV711 (M290)	BD Biosciences	Cat#564320; RRID:AB_2738743
CD69 APC (H1.2F3)	Biolegend	Cat#104514; RRID:AB_492843
CD69 BV650 (H1.2F3)	BD Biosciences	Cat#740460; RRID:AB_2740186
CD44 PE-Cy7 (IM7)	Biolegend	Cat#103030; RRID:AB_830787
PD-1 AF647 (29F.1A12)	Biolegend	Cat#135230; RRID:AB_2566008
CXCR5 PE (L138D7)	Biolegend	Cat#145504; RRID:AB_2561968
CD62L PE (MEL-14)	Biolegend	Cat#104408; RRID:AB_313095
IFNγ APC (XMG1.2)	BD Biosciences	Cat#554413; RRID:AB_398551
IL10 PEcy7 (JES5-16E3)	Biolegend	Cat#505026; RRID:AB_11150582
IL17A PE (ebio17B7)	Thermo Fisher Scientific	Cat#12-7177-81; RRID:AB_763582
TNF BB700 (MP6-XT22)	BD Biosciences	Cat#566510; RRID:AB_2869775
RORγt BV786 (Q31-37)	BD Biosciences	Cat#564723; RRID:AB_2738916
FOXP3 eflour450 (FJK-16s)	Thermo Fisher Scientific	Cat#48-5773-82; RRID:AB_1518812
Tbet APC (4B10)	Biolegend	Cat#644814; RRID:AB_10901173
GATA3 PerCP-eFluor710 (TWAJ)	Thermo Fisher Scientific	Cat#46-9966-42; RRID:AB_10804487
EpCAM PerCp/Cy5.5 (G8.8)	Biolegend	Cat#118220; RRID:AB_2246499
EpCAM BV605 (G8.8)	Biolegend	Cat#118227; RRID:AB_2563984
CD19 BUV563 (1D3)	BD Biosciences	Cat#749028; RRID:AB_2873425
CD38 BB700 (90/CD38)	BD Biosciences	Cat#742132; RRID:AB_2871393
CD95 BV750 (Jo2)	BD Biosciences	Cat#747413; RRID:AB_2872101
GL7 PerCP/Cy5.5 (GL7)	Biolegend	Cat#144610; RRID:AB_2562979
NK1.1 BV605 (PK136)	Biolegend	Cat#108753; RRID:AB_2686977
NK1.1 BV570 (PK136)	Biolegend	Cat#108733; RRID:AB_10896952
CD11c BV605 (N418)	Biolegend	Cat#117334; RRID:AB_2562415
TER119 BV605 (TER-119)	Biolegend	Cat#116239; RRID:AB_2562447
F4/80 BV605 (BM8)	Biolegend	Cat#123133; RRID:AB_2562305
CD3ε BV605 (145-2C11)	Biolegend	Cat#100351; RRID:AB_2565842
Ly-6G BV605 (1A8)	Biolegend	Cat#127639; RRID:AB_2565880
B220 APC/Fire 810 (RA3-6B2)	Biolegend	Cat#103277; RRID:AB_2860603
IgA PE goat polyclonal	SouthernBiotech	Cat#1040-09; RRID:AB_2794375
IgA 488 goat polyclonal	SouthernBiotech	Cat#1040-30; RRID:AB_2794376

(*Continued on next page*)

Continued

REAGENT or RESOURCE	SOURCE	IDENTIFIER
IgA BIOT goat polyclonal	SouthernBiotech	Cat#1040-08; RRID:AB_2794374
IgD BV421 (11-26c.2a)	Biolegend	Cat#405725; RRID:AB_2562743
IgD BV605 (11-26c.2a)	Biolegend	Cat#405727; RRID:AB_2562887
IgM BUV661 (II/41)	BD Biosciences	Cat#750660; RRID:AB_2874787
TotalSeq-C0301 anti-mouse Hashtag 1 (M1/42)	Biolegend	Cat#155861; RRID:AB_2800693
TotalSeq-C0302 anti-mouse Hashtag 2 (M1/42)	Biolegend	Cat#155863; RRID:AB_2800694
TotalSeq-C0303 anti-mouse Hashtag 3 (M1/42)	Biolegend	Cat#155865; RRID:AB_2800695
TotalSeq-C0304 anti-mouse Hashtag 4 (M1/42)	Biolegend	Cat#155867; RRID:AB_2800696
TotalSeq-C0305 anti-mouse Hashtag 5 (M1/42)	Biolegend	Cat#155869; RRID:AB_2800697
TotalSeq-C0306 anti-mouse Hashtag 6 (M1/42)	Biolegend	Cat#155871; RRID:AB_2819910
Bacterial and virus strains		
Murine Astrovirus	This paper	UofC1
Murine Astrovirus	Gift from Dr. Cadwell K. (University of Pennsylvania, Philadelphia, PA, USA)	NYU1
Norovirus MNV-CR6	Gift from Wobus C. (University of Michigan, Ann Arbor, MI, USA)	MNV-CR6
Norovirus MNV-CR3	Gift from Wobus C. (University of Michigan, Ann Arbor, MI, USA)	MNV-CR3
Reovirus, strain T1L	Gift from Dermody T.S. (University of Pittsburgh, Pittsburgh, PA, USA)	T1L
Rotavirus, strain EDIM	Gift from Altan-Bonnet N. (NIH, Bethesda, MD, USA)	EDIM
Biological Samples		
Fetal Bovine Serum	Biowest	Cat#S01520
Normal Goat Serum	JacksonImmunoResearch	Cat#005-000-121
Normal Rat Serum	JacksonImmunoResearch	Cat#012-000-120
Chemicals, Peptides, and Recombinant Proteins		
Corning™ RPMI 1640 with L-Glutamine	Fisher Scientific	Cat#MT-10043CV
EDTA, 0.5M, pH8.0	Thermo Fisher Scientific	Cat#AM9260G
1M MgCl2	Thermo Fisher Scientific	Cat#AM9530G
Collagenase from Clostridium histolyticum	Sigma-Aldrich	Cat#C2139
Cytiva Percoll™ Centrifugation Media	Fisher Scientific	Cat#45-001-747
Phorbol Myristate Acetate	Sigma-Aldrich	Cat#P1585
Ionomycin Calcium Salt from Streptomyces conglobatus	Sigma-Aldrich	Cat#10634
BD GolgiStop Protein Transport Inhibitor	BD Biosciences	Cat#554724
Ampicillin sodium salt	Sigma-Aldrich	Cat#A9518
Vancomycin hydrochloride	Sigma-Aldrich	Cat#V2002
Neomycin trisulfate salt	Sigma-Aldrich	Cat#N1876
Metronidazole	Sigma-Aldrich	Cat#M1547
Emtricitabine	Fisher Scientific	Cat#AC462070050
Tenofovir	Fisher Scientific	Cat#AC461250250
Acyclovir	Fisher Scientific	Cat#A19151G
Lamivudine	Fisher Scientific	Cat#L02171G
Ribavirin	Fisher Scientific	Cat#R0077500MG
RNAprotect Tissue Reagent	Qiagen	Cat#76106
2-Mercaptoethanol	Sigma-Aldrich	Cat#M3148
Ethanol 200 Proof	Decon Labs Inc	Cat#DSP-MD 43
Inhibitex Buffer	Qiagen	Cat#19593

(*Continued on next page*)

Continued

REAGENT or RESOURCE	SOURCE	IDENTIFIER
Cytiva HyClone™ Water	Fisher Scientific	Cat#SH3053801
10% Formalin Solution	Sigma-Aldrich	Cat#HT501128
Paraformaldehyde	Sigma-Aldrich	Cat#158127
Sucrose	Sigma-Aldrich	Cat#S9378
Triton X-100	Sigma-Aldrich	Cat#X100
O.C.T. Compound	Sakura	Cat#4583
Critical Commercial Assays		
SytoBC	Thermo Fisher Scientific	Cat#S34855
LIVE/DEAD® Fixable Aqua Dead Cell Stain Kit	Thermo Fisher Scientific	Cat#L34966
Zombie NIR™ Fixable Viability Kit	Biolegend	Cat#423106
BD Cytofix/Cytoperm Plus Fixation/Permeabilization Solution Kit	BD Biosciences	Cat#554714
eBioscience™ Foxp3 / Transcription Factor Staining Buffer Set	Thermo Fisher Scientific	Cat#00-5523-00
QIAamp Fast DNA Stool Mini Kit	Qiagen	Cat#51604
QX200 ddPCR EvaGreen Supermix	Bio-Rad	Cat#1664034
Qubit dsDNA High Sensitivity	Thermo Fisher Scientific	Cat#20018794
Illumina DNA Prep	Illumina	Cat#20018704
RNeasy Plus Mini Kit	Qiagen	Cat#74136
RNeasy Micro Kit	Qiagen	Cat#74004
High-Capacity cDNA RT kit	Thermo Fisher Scientific	Cat#4368814
SuperScript™ VILO cDNA kit	Thermo Fisher Scientific	Cat#11754050
TB Green Advantage qPCR Premix	Takara	Cat#639676
Power SYBR™ Green RNA-to-C_T 1-Step kit	Fisher Scientific	Cat#50-591-795
Smart-Seq® v4 Ultra® low Input RNA kit	Takara	Cat#634889
Nextera XT DNA Library Preparation Kit	Illumina	Cat#FC-131-1001
TruSeq® Stranded mRNA Library Prep	Illumina	Cat#20020595
TruSeq® RNA CD Index Plate	Illumina	Cat#20019792
SuperScript™ II RT	Thermo Fisher Scientific	Cat#18064071
AMPure XT	Beckman Coulter	Cat#A63881
KAPA library quantification kit	Roche	Cat#07960140001
ProLong™ Diamond Antifade Mountant with DAPI	Thermo Fisher Scientific	Cat#P36962
Pierce™ Protein L Magnetic Beads	Thermo Fisher Scientific	Cat#88850
IgA mouse Uncoated ELISA kit	Thermo Fisher Scientific	Cat#88-50450-86
IgM mouse Uncoated ELISA kit	Thermo Fisher Scientific	Cat#88-50470-76
Deposited data		
16s rRNA sequencing	This study	PRJNA1212528
Metagenomic sequencing	This study	PRJNA1212528
Bulk RNA sequencing	This study	GEO: GSE289554, GSE289553
Single cell RNA sequencing	This study	GEO: GSE289917
Experimental models: Organisms/strains		
Mouse: C57BL/6J Ighasec-/-	This study	N/A
Mouse: C57BL/6J Igha-/-	This study	N/A
Mouse: C57BL/6J Jh-/-	This study	N/A
Mouse: B6.129S(C)-*Batf3*^{tm1Kmm}/J	Jackson laboratory	Strain #:013755; RRID:IMSR_JAX:013755
Mouse: B6.129P2-*H2-K1*$^{b\text{-}tm1Bpe}$*H2-D1*$^{b\text{-}tm1Bpe}$/DcrJ	Jackson laboratory	Strain #:019995; RRID:IMSR_JAX:019995

(*Continued on next page*)

Continued

REAGENT or RESOURCE	SOURCE	IDENTIFIER
Mouse: B6.129P2-*B2m*^{tm1Unc}/DcrJ	Jackson laboratory	Strain #:002087;RRID:IMSR_JAX:002087
Mouse: B6.129P2-*Il10*^{tm1Cgn}/J	Jackson laboratory	Strain #:002251; RRID:IMSR_JAX:002251
Oligonucleotides		
GAPDH Forward 5′-AGGTCGGTGTGAACGGATTTG-3′	Abadie et al.[50]	N/A
GAPDH Reverse 5′-TGTAGACCATGTAGTTGAGGTCA-3′	Abadie et al.[50]	N/A
ORF1b Forward 5'-TACATCGAGCGGGTGGTCGC-3'	Yokoyama et al.[31]	N/A
ORF1b Reverse 5'-GTGTTACTAACGCGCACCTTTTCA-3'	Yokoyama et al.[31]	N/A
MNV Forward 5'-ATGGTRGTCCCACGCCAC-3'	Bouziat et al.[51]	N/A
MNV Reverse 5'-TGCGCCATCACTCATCC-3'	Bouziat et al.[51]	N/A
T1L S4 83 Forward: 5'-CGCTTTTGAAGGTCGTGTATCA-3'	Bouziat et al.[51]	N/A
T1L S4 153 Reverse: 5'-CTGGCTGTGCTGAGATTGTTTT-3'	Bouziat et al.[51]	N/A
NSP5 Forward: 5′-CTGCTTC AAACGATCCACTCAC-3′	Hou et al.[52]	N/A
NSP5 Reverse: 5'-TGAATCCATAGACACGCC-3′	Hou et al.[52]	N/A
18S rRNA Forward 5'-GTTCCGACCATAAACGATGCC-3'	Blanchet et al.[53]	N/A
18S rRNA Reverse 5'-GTTCCGACCATAAACGATGCC-3'	Blanchet et al.[53]	N/A
V4 16S rRNA 519 Forward 5'-CAGCMGCCGCGGTAA-3'	Burggraf et al.[54]	N/A
V4 16S rRNA 806 Reverse 5'-GGACTACHVG GGTWTCTAAT-3'	Caporaso et al.[55]	N/A
Universal Mouse Reference RNA	Thermo Fisher Scientific	Cat#QS0640
Software and Algorithms		
QIIME2: 2022.8.0	Bolyen et al.[56]	https://github.com/qiime2
Silva (v138)	Quast et al.[57]	https://www.arb-silva.de
SciPy (v1.7.3)	Virtanen et al.[58]	https://www.scipy.org/
Statsmodels (v0.13.2)	Seabold and Perktold[59]	https://www.statsmodels.org/stable/index.html
Python 3.7.6	Phyton Software Foundation	https://www.python.org/
KneadData (v0.12.0)	Huttenhower Lab	https://github.com/biobakery/kneaddata
MetaPhlAn4 (v4.0.3)	Blanco-Míguez et al.[60]	https://github.com/biobakery/MetaPhlAn
R (v.4.2.2)	R Core Team	https://www.r-project.org
GraphPad Prism 10	GraphPad	https://www.graphpad.com
FlowJo	TreeStar	https://www.flowjo.com
QuPath	Bankhead et al.[61]	https://qupath.github.io
Other		
Bead Ruptor Elite bead mill homogenizer	Omni International	Cat#19-040E
Zirconium Oxide Beads 0.5 mm RNA Free	Next Advance	Cat#ZROB05-RNA
Zirconium Oxide Beads 1.0 mm RNA Free	Next Advance	Cat#ZROB10-RNA
BioSpec 0.1 mm Glass Beads	Fisher Scientific	Cat#NC0268065
BioSpec 1.0 mm Zirconia/Silica Beads	Fisher Scientific	Cat#NC9847287
LightCycler® 480 System	Roche	N/A
Cytek® Aurora	Cytek	N/A
CRi Pannoramic SCAN 40x Whole Slide Scanner	3DHistech	N/A
VS200 Slideview Research Slide Scanner	Olympus	N/A
EasyEights™ EasySep™ Magnet	StemCell technologies	Cat#18103
QX200 ddPCR system	BioRad	Cat#1864001

EXPERIMENTAL MODELS AND STUDY PARTICIPANT DETAILS

Mice

Batf3-/- (Strain #:013755),[25] B2m-/- (Strain #:002087)[62] and K^bD^b-/- (Strain #:019995),[63] IL10-/- (Strain #:002251)[64] mice were purchased from The Jackson Laboratory and crossed to *Ighasec*-/- mice to generate double or triple knock-out lines. B cell deficient mice lacking IgH J locus, JH-/-, were generated using Cas9 and protospacers GCTACTGGTACTTCGATGTC and GCCATTCTTACCTGAGGAGA. Classical IgA deficient line, Igha-/-, lacking IgA switch region (Sα) and 5' fragment of the C1α exon was generated using Cas9 and protospacers AAGCGGCCACAACGTGGAGG and TCAAGTGACCCAGTGATAAT. Secretory IgA deficient line, Ighasec-/-, lacking secretory tailpiece and downstream secretory polyadenylation signal (CSα + polyA) was generated using Cas9 and protospacers TGTCTGTGATCATGTCAGA and GGGGCCATCTCAAGAACTGC. JH-/-, IgA deficient mice and IL10-/- were rederived germ-free (GF) at Taconic Biosciences. GF mice were housed in gnotobiotic isolators at University of Chicago Gnotobiotic Research Animal Facility and routinely screened for sterility by culture or 16S rRNA gene qPCR. Some GF *Ighasec*+/- and *Ighasec*-/- mice were monocolonized with NYU1 MuAstV. Bcl6 $^{fl/fl}$ CD4^{Cre} and Bcl6 $^{fl/fl}$ CD21^{Cre} mice were obtained from Jason G. Cyster and were housed at UCSF animal facility. For experiments, littermates were used at 8-12 weeks of age unless specified otherwise. Mice were fed a standard chow diet. Animal husbandry and experimental procedures were performed in accordance with Public Health Service policy and approved by the University of Chicago Institutional Animal Care and Use Committee.

Antibiotic and antiviral treatments

6-8-week-old Ighasec+/- and Ighasec-/- mice were provided ampicillin (1g L^{-1}), vancomycin (0.5g L^{-1}), neomycin (1g L^{-1}), and metronidazole (1g L^{-1}) in drinking water for four weeks as described previously.[65] In some experiments, combination of metronidazole and vancomycin, or singular antibiotic was provided to the mice for the duration of the treatment. All antibiotics were purchased from Sigma.

Anti-retroviral and anti-viral drug cocktails were administered daily to 4-week-old Ighasec+/- and Ighasec-/- mice for 4 weeks by oral gavage as described previously.[28,29] Anti-retroviral treatment consisted of 100 mg kg^{-1} of tenofovir (Arcos Organics) and 60 mg kg^{-1} emtricitabine (Fisher Scientific). Anti-viral treatment consisted of 30 mg kg^{-1} acyclovir (Fisher Scientific), 10 mg kg^{-1} lamivudine (Fisher Scientific) and 30 mg kg^{-1} and ribavirin (Fisher Scientific).

Viral infections

Viruses were administered to 4–6-week-old GF *Ighasec*+/- and *Ighasec*-/- mice by oral gavage. EDIM was a gift from N. Altan-Bonnet (NIH]. Dose administered was 10^4 plaque forming units (PFU) of EDIM as described previously.[66] MNV-CW3 and MNV-CR6 were a gift from C. Wobus (University of Michigan Medical School). Mice were infected with 3x10^6 PFUs of MNV-CW3 or MNV-CR6 as described previously.[67] T1L reovirus was obtained from T.S. Dermody (University of Pittsburgh). Mice were inoculated with 10^8 PFU of T1L.[68] MuAstV was purified from fecal pellets of broad-spectrum antibiotic-treated *Ighasec*-/- mice. Briefly, 4–6 fecal pellets were collected into sterile bead-beating tube containing 1.0 mm zirconia/silica beads (Fisher Scientific). Homogenization was performed after adding 1 mL of sterile PBS using Bead Ruptor Elite mill homogenizer (Omni) at a speed of 5 m/s for 1 min. Homogenates were centrifuged at 17000g for 5 min at 4°C to pellet the beads and fecal matter. Supernatants were collected and centrifuged at 17000g for 5 min at 4°C. This step was repeated twice to remove any remaining debris. 400 μL of the supernatant was collected from the top and diluted tenfold. Solution was filtered through 0.22 μm syringe-driven filter unit (Millipore Sigma). Filtration step was repeated three times. Virus stock was aliquoted and stored at -80°C. Virus titer was quantified as genome copy per μL by qPCR. Pure stock of NYU1 MuAstV was obtained from K. Cadwell (NYU). Mice were inoculated with 10^9 genome copies/mouse of the MuAstVs used.[67]

Microbial transfers

To colonize GF Ighasec+/- and Ighasec-/- mice with microbiota, 3-4 fresh fecal pellets were collected from ASF donor mouse purchased from Taconic Biosciences, C57BL6/J purchased from Jackson Laboratories, Ighasec-/- housed in UofC Barrier I or Barrier II facilities or 13-species donor mouse provided by M. Mimee (University of Chicago). Feces were homogenized in 1mL of sterile PBS on a vortex for 3 min and centrifuged at 300 g for 5 min at 4°C to remove debris. 200 μL of the supernatant was administered to recipient mice by oral gavage. To colonize mice with fecal filtrate, feces were collected from vancomycin/metronidazole treated Ighasec-/- mouse. Homogenate was prepared as described above. After debris removal, collected supernatant was centrifuged at 8000g for 10 min at 4°C to pellet any bacteria. Supernatant was then filtered three times through 0.22 μm syringe-driven filter unit (Millipore Sigma). An aliquot of the filtrate was treated with 50mJ/cm^2 of UV light using Spectrolink XL-1000 UV crosslinker (Spectroline).[69] 200 μL of the filtrate was administered to recipient mice by oral gavage. To colonize mice with the *L. reuteri*, sequenced strain isolated from vancomycin/metronidazole treated mice was used. Single colony grown on MRS agar (Fisher Scientific) was picked to inoculate 10 mL of MRS broth (Fisher Scientific) and cultured anaerobically for 16-18h at 37°C. Bacteria were then pelleted, washed, and re-suspended in 3 mL of sterile PBS. 200 μL of the supernatant was administered to recipient mice by oral gavage. For all the microbial transfers, mice were colonized at 4-weeks of age and euthanized at 8 weeks of age.

DSS-induced colitis

2% or 2.5% DSS (MW ca 40000, Thermo Scientific) in water was administered to *Ighasec*+/- and *Ighasec*-/- mice housed in UofC Barrier I or UofC Barrier II previously infected with MNV-CR6 respectively. Mice were kept on DSS water for seven days, followed

by regular water for two days and euthanized. Weight was recorded every day throughout the duration of the DSS protocol. Bacterial translocation to mLNs, colon length and histology was assessed. To determine the extent of bacterial translocation, mLNs were dissected aseptically, weighed, and homogenized with Tissue-Tearor rotor (BioSpec) in 500 μL of sterile PBS. 250 μL of homogenate was plated in duplicate on Brucella agar with 5% sheep blood hemin and vitamin K (BD) and cultured anaerobically (48h) at 37°C. Colony forming units were counted and normalized to the weight (g) of the dissected tissue.

METHOD DETAILS

Isolation of intraepithelial and lamina propria lymphocytes

Intestines were excised and divided into segments as previously described.[9] 12 cm of duodenum (measured from the pyloric sphincter), jejunum (measured from the middle), ileum (measured from the ileocecal valve) and entire colon (from the cecum to the rectum) were collected to isolate the immune cells for flow cytometry. In the small intestinal segments, any Peyer's patches were removed and discarded. Segments were opened longitudinally and washed in phosphate-buffered saline (PBS) to remove mucus and any fecal matter. Intestines were then cut into 1cm pieces. IELs and LP lymphocytes were isolated as previously described[70] using EDTA-containing calcium-free media and collagenase VIII (Sigma-Aldrich, C2139), respectively. To remove debris, cells isolated from IEL and LP fractions were resuspended in 10 mL of 40% Percoll (GE Healthcare) and centrifuged as previously described.[50] Pelleted cells from IEL and LP fractions were washed in PBS supplemented with 2% fetal bovine serum and counted.

Single cell tissue suspensions

Peyer's patches (PP) and mesenteric lymph nodes (mLNs) were excised and incubated in RPMI supplemented with 10% fetal bovine serum (FBS) and collagenase VIII (Sigma-Aldrich, C2139) at 37 °C for 30 min. Digested tissues were pressed through 70 μm cell strainer (Corning) to obtain single cell suspensions and quantified.

Ex-vivo cell stimulation

Up to $2.5x10^6$ of isolated cells were used for ex-vivo stimulation to determine cytokine production. Cells were resuspended in RPMI supplemented with 10% FBS incubated for 2 h (37°C with 5% CO_2) in 48-well plates in presence of ionomycin (750 ng mL^{-1}, Sigma-Aldrich), phorbol 12-myristate 13-acetate (50 ng mL^{-1}, Sigma-Aldrich) and Golgi stop (BD). After incubation, the stimulation was quenched on ice with ice-cold FACS buffer (PBS with 2% FBS), cells were harvested and stained for flow cytometry.

Flow cytometry

Cells were incubated with Fc-block (CD16/32) for 10 min at 4°C to prevent any non-specific binding, followed by staining with dead dye (LIVE/DEAD Aqua, Thermo Fisher or Zombie NIR, Biolegend) for 15 min at 4°C to determine cell viability. Cells were then incubated with antibodies detecting cell surface antigens for 20 min at 4°C. BD Cytofix/Cytoperm kit was used for intracellular cytokine staining. Briefly, after cell surface staining, cells were fixed in the dark for 20 min at 4°C in fixation/permeabilization solution, washed, and incubated with antibodies detecting intracellular cytokines in Perm/Wash buffer for 40 min at 4°C. eBioscience Foxp3 / Transcription Factor Staining Buffer Set was used for intracellular transcription factor staining according to manufacturer instructions. All antibodies used in the study are listed in the key resources table. The cells were acquired on Cytek Aurora (Cytek Biosciences) or sorted on Symphony S6 (BD Biosciences), and recorded events were analyzed using FlowJo (BD Biosciences). In all experiments, the cells were pre-gated as follows: FSC, SSC, singlets, and live. CD8αβ$^+$ IELs were gated CD45$^+$, TCRβ$^+$, CD4$^-$, CD8α$^+$, CD8β$^+$. T_{FH} cells were gated CD45$^+$, TCRβ$^+$, CD4$^+$, CD8α$^-$, CD44^{hi}, CXCR5$^+$, PD-1$^+$. GC B cells were gated CD45$^+$, CD19$^+$,TCRβ$^-$, CD38$^-$, CD95$^+$/GL7$^+$. IgA plasma cells were gated as described previously,[1] EpCAM$^-$, CD45$^{+/lo}$, lineage negative (Ter119$^-$, F4/80$^-$, CD3$^-$, Ly6G$^-$, NK1.1$^-$, CD19$^-$), IgA$^+$, B220$^-$. Intestinal epithelial cells (IECs) were gated CD45$^-$ EpCAM$^+$. For downstream RNAseq analysis, 50000 IECs from the jejunum and ileum were sorted into RLT buffer (Qiagen) supplemented with 2-mercaptoethanol (Sigma-Aldrich).

Bacterial flow cytometry

Small and large intestinal luminal contents were taken from WT, Igha-/- and Ighasec-/- mice and resuspended at a concentration of 0.1mg/μl in 1X PBS supplemented with protease inhibitors (Cell signaling). Luminal contents were then homogenized on a vortex for 5 min. Fecal debris was pelleted at 400 g for 5 min. The supernatant was collected and centrifuged at 8000 g to pellet bacteria. The bacteria were then washed, pelleted, and stained with SYTO BC (ThermoFisher) followed by anti-IgA PE (Southern Biotech) and anti-IgM AF647 (Southern Biotech). Bacteria were gated FSC, SSC, SYTOBC$^+$, and IgA$^+$/IgM$^+$.

In-vivo cell depletion

To deplete CD8αβ$^+$ IELs, mice were injected intraperitoneally with 250 μg of anti-CD8β monoclonal antibody (Bio X Cell, 53-5.8, Rat IgG1) for three weeks every other day. To deplete CD4 T cells, mice were injected intraperitoneally with 250μg of anti-CD4 monoclonal antibody (Bio X Cell, GK1.5, Rat IgG2b) for four weeks every three days. Control animals were injected with corresponding isotype antibodies (Bio X Cell, HRPN, Rat IgG1 or LTF-2, Rat IgG2b) for the duration of the depletion studies. Efficacy of the depletion was confirmed by flow cytometry using anti-CD8β (BD Biosciences, H35-17.2) or anti-CD4 (Biolegend, RM4-4) antibodies.

ELISA

Serum IgA or IgM levels were assessed using IgA mouse uncoated ELISA kit (Thermo Fisher) or IgM mouse uncoated ELISA kit (Thermo Fisher) according to manufacturer's protocol. Serum was serially diluted in 1x Assay Buffer A (Thermo Fisher). Dilution in the middle of standard curve was used to quantify IgA or IgM levels. Absorbance was read at 450 nm.

Histology

7-10 cm of duodenum, jejunum and ileum or whole colon were excised, cleaned of adipose tissue, and opened longitudinally. Intestinal content was removed. Starting from the most distal end and with the luminal side facing upwards, tissues were rolled into Swiss rolls. Tissue was then placed into histology cassettes and fixed with 10% formalin (Sigma-Aldrich) for H&E staining or with 4% PFA in PBS (Sigma-Aldrich) for immunofluorescence staining. Formalin fixed tissues were transferred into 70% ethanol, embedded in paraffin, and cut at 5 μm thickness. Paraffin embedding, tissue processing and H&E staining was performed by the Human Tissue Resource Center at the University of Chicago. Scoring of the H&E-stained colonic tissue was performed using parameters determined by Dr. Christopher Weber. Briefly, the entire length of the colon Swiss roll was measured using QuPath.[61] Then sections of the mucosa were scored and measured based on appearance: 0- normal appearance, 1- mild edema, increased lamina propria lymphocytes and attenuation of epithelium without ulceration, 2- severe epithelial regeneration with signs of healed erosion, high immune cell infiltration and edema; 3- Severe edema, complete ulceration, and high inflammatory infiltration. Final score was calculated as a proportion of severely affected tissue versus the total length of the tissue.

PFA fixed tissues were rinsed with PBS and transferred into 30% sucrose solution (Sigma-Aldrich) and incubated overnight at 4°C. Cryopreserved tissues were then embedded in O.C.T. Compound (Sakura), frozen and stored at -80°C. Frozen tissues were cut at 5 μm thickness, dried and stored at -20°C until processing. Frozen tissue sections were permeabilized with 0.1% Triton X-100 (Sigma-Aldrich) in PBS, blocked in buffer containing normal rat and goat sera (Jackson Immuno Research) and stained overnight at 4°C. Antibodies used for immunofluorescence staining were anti-mouse CD8β Alexa Fluor 647 (Biolegend), and IgA Alexa Fluor 488 (Southern Biotech). The slides were then washed three times with permeabilization buffer, briefly rinsed in water, and mounted with ProLong Diamond Antifade with DAPI (Thermo Fisher). The slides were imaged with the CRi Pannoramic SCAN 40x Whole Slide scanner or Olympus VS200 Slideview Research Slide Scanner at the University of Chicago Integrated Light Microscopy core.

DNA isolation

50-100 mg of the intestinal contents were collected from the middle 5cm of the jejunum, the last 5 cm of ileum, and the middle 5cm of the colon. Contents were transferred into 2mL screw-cap tube containing 0.1 mm BioSpec glass beads (Fisher Scientific), snap frozen on dry ice and stored at -80°C. Intestinal contents were homogenized in 1mL of InhibitEX buffer (Qiagen) using the Bead Ruptor Elite Bead mill homogenizer (Omni) on speed 6m/s for 3 min. DNA was purified from the lysates using QIAmp Fast DNA stool kit (Qiagen) according to manufacturer's protocol. DNA concentration was determined using the nanodrop UV spectrophotometer (ThermoFisher) or Qubit dsDNA Quantification Assay (ThermoFisher).

Microbial 16S rRNA Gene Sequencing

Extracted DNA was quantified, amplified, barcoded, sequenced, filtered, and analyzed as described previously.[9,71,72] Briefly, total absolute bacterial load was obtained with dPCR using the QX200 ddPCR system (Bio-Rad) with primers targeting the variable 4 (V4: 519F-806R) region of the 16S rRNA gene. For library preparation, 500 ng total DNA (determined by NanoDrop) was used to amplify the V4 region of 16S rRNA gene with barcoded primers. Obtained libraries were quantified with KAPA library quantification kit (Roche), normalized, multiplexed, and sequenced at average depth of 157,552 (2x300 bp) on an Illumina MiSeq v3 (Illumina).

Microbial DNA Shotgun Sequencing

200 ng of purified fecal DNA (determined by Qubit dsDNA High Sensitivity kit) was used to prepare libraries for metagenomic sequencing with Illumina DNA Prep kit (Illumina). Library was sequenced on an Illumina NovaSeq6000 S4 (2x150bp) with a read depth of 264 million reads.

IgA-MuAstV pulldown

2-3 fresh fecal pellets were collected from GF or MuAstV monoassociated Ighasec+/- mice to pull-down IgA. Feces were homogenized in 500 μL 1X Tris-Buffered Saline, 0.1% Tween 20 (TBST) on a vortex for 5 min, and centrifuged for 5 min at 8000 g, 4°C. The supernatant was collected and centrifuged twice to remove any remaining debris. Pierce Protein L Magnetic Beads (Thermo Fisher) were added to the supernatants and incubated at room temperature with agitation for 1h. Beads were collected using EasySep magnetic stand (StemCell technologies) to pull down the IgA through kappa light chain. Supernatant was saved for downstream RNA isolation. Beads were washed three times with TBST, collected and incubated with RLT Plus buffer (Qiagen) supplemented with 2-mercaptoethanol. RNA from obtained lysates was purified using RNeasy Micro kit (Qiagen) according to manufacturer's specifications. 10 μL of obtained RNA was reverse transcribed to cDNA using SuperScript VILO cDNA kit. cDNA obtained from the supernatant and the bead-bound fraction was used to determine the number of MuAstV copies per reaction via qPCR.

RNA isolation

1 cm of tissue from the beginning of the duodenum, the middle of the jejunum, the end of the ileum, and the middle of the colon was excised and preserved in RNAprotect (Qiagen) overnight at 4°C. The preserved tissue was then stored at -80°C until processing. Tissue was thawed on ice and transferred to a screw-cap tube containing 450 μL of RLT Plus buffer supplemented with 2-mercaptoethanol and equal quantities of 1.0mm and 0.5 mm zirconium oxide beads (Next Advance). Tissue was homogenized three times for 30 sec at a speed of 6 m/s using Bead Ruptor Elite mill homogenizer (Omni), with 1 min incubation on ice between each cycle. RNA from the lysates was purified using RNeasy Plus Mini kit (Qiagen) with the optional on-column DNase I digest step according to manufacturer protocol.

qPCR

1 μg of RNA was reverse transcribed to cDNA using High-Capacity cDNA RT kit (Thermo Fisher) according to manufacturer's protocol. 10 ng of cDNA was used to measure the expression of the genes of interest via qPCR with TB Green Advantage qPCR Premix (Takara) on a Light Cycler 480 (Roche). The expression of the genes of interest was quantified and normalized to GAPDH using $1000*2^{-(Ct\ target-\ Ct\ housekeeping)}$ formula. To calculate the number of MuAstV copies per reaction, linearized plasmid standard curve was used. Primer pairs used in the study are listed in key resources table.

RNA-seq library preparation

RNA was purified as detailed above from jejunal and ileal tissue of anti-CD8β, or isotype treated *Ighasec*+/- and *Ighasec*-/- mice. 500 ng of RNA was used as input in the TruSeq Stranded mRNA Library Prep (Illumina) according to manufacturer's specifications.

50000 $CD45^-EpCAM^+$ IECs were sorted from the jejunum and the ileum of anti-CD8β, or isotype treated *Ighasec*+/- and *Ighasec*-/- mice. Two independent sorting experiments were performed. Cells were collected into RLT Plus buffer (Qiagen) supplemented with 2-mercaptoethanol. RNA was purified using RNeasy Micro kit (Qiagen) and quantified with Power SYBR™ Green RNA-to-C_T 1-Step kit. The SMART-Seq v4 Ultra Low input RNA kit (Takara) was used to generate cDNA from 10 ng of RNA. cDNA was amplified 9 cycles and purified according to manufacturer's protocol. 200 pg of purified cDNA was the used to generate RNA-seq libraries with Nextera XT DNA Library preparation kit (Illumina).

Obtained libraries were quantified with KAPA library quantification kit (Roche), normalized, multiplexed, and sequenced at a depth of 20 million reads per sample (100 bp) on a NovaSEQ-6000 (Illumina) at the University of Chicago Genomics Facility.

Single cell RNA-seq

$CD8\alpha\beta^+$ IELs from three Ighasec+/- and Ighasec-/- mice were isolated and stained as described above in "flow cytometry" section. For cell hash-tagging, TotalSeq-A™ hashtag antibodies (key resources table) were added to each sample individually during the cell surface staining. The samples were then sorted together directly into FACS buffer, spun down and reconstituted in 1X PBS (calcium- and magnesium-free) containing 0.04% BSA. Samples were loaded on 10x Chromium Controller (10x Genomics) immediately after sorting. Libraries were constructed for gene expression data and TCR repertoire using Chromium Next GEM Single Cell 5' Library kit (v1.1). Capture, library preparation and sequencing were performed at the University of Chicago Genomics Facility.

QUANTIFICATION AND STATISTICAL ANALYSIS

Statistical analyses were performed using GraphPad Prism software. Two-tailed unpaired Student's t-test and one-way ANOVA with Turkey multiple comparisons test were used for normally distributed data with two or multiple comparisons respectively. Mann-Whitney U test was used for non-normally distributed data. Prolapse incidence curves were generated using Kaplan-Meier estimate and analyzed using the log-rank (Mantel-Cox) test. All the data is represented as a mean with standard error of the mean (SEM). The statistical significance was defined as **** $P<0.0001$, *** $P<0.001$, ** $P<0.01$, * $P<0.05$ ns $P \geq 0.05$ or °°° $P<0.001$, °° $P<0.01$, ° $P<0.05$. Number (n) of animals per study and statistical tests used are detailed in the figure legends.

Analysis of Microbial 16S rRNA Gene Sequencing and Microbial DNA Shotgun Sequencing

Sequences of V4 region of 16S rRNA were processed with QIIME 2 (v2022.8.0) and SILVA (v138) for taxonomy assignment. Reads were rarefied to 55,000 reads based on the lowest read depth sample. For bacterial absolute abundance measurements, the relative abundance of each taxon was multiplied by the total microbial load in the sample. Filtering of low abundance taxon was performed by calculating the LOD based on 1. the number of 16S rDNA molecules input into the library preparation and 2. the number of sequencing reads. The minimum of the two LOD calculations was used and any ASV detected below the LOD was set to 0. Statistical comparisons were performed with the non-parametric Kruskal-Wallis rank sums tests with Benjamini–Hochberg multiple hypothesis testing correction using SciPy (v1.7.3) and statsmodels (v0.13.2).

DNA shotgun sequencing QC and host filtering was performed with KneadData (v0.12.0) using the mouse reference genome (C57BL/6J). For marker-gene taxonomic analysis, host filtered sequences were analyzed with MetaPhlAn4 (v4.0.3). To determine all organisms present, k-mer analysis was performed on the host filtered sequences using Kraken2 (v2.1.3) with the entire NT database (last updated 11/29/2023) with a confidence threshold of 0.5. Reads assigned to species identified as less than 0.01% abundance were filtered out for the final read distribution. Reads assigned to the fungal kingdom and viral domain were retained to highlight the low abundance of non-bacterial microbial reads.

Recovery of viral reads from the bulk RNA-seq

Reads were assembled into contigs using Megahit,[73] and contigs were aligned to the nr protein database from NCBI using DIAMOND.[74] Representative full genome sequences of Murine Astrovirus 1 were downloaded from NCBI Genbank, and a STAR[75] alignment database was constructed out of those full genome sequences. Reads were then aligned to the full genomes using STAR. Recovered reads were normalized as follows: (#MuAstV reads/#reads total)10^6.

Mouse bulk RNA-seq data analysis: Quality control filtering and normalization

All statistical analyses of the mouse RNA-seq data were performed using R (v.4.2.2). From the raw count matrices, genes expressed (i.e., having at least two counts) in fewer than two samples were removed. The resulting matrices will be referred to as the count matrices. Counts were normalized by applying the variance stabilizing transformation (i.e. vst(), default parameters) from the DESeq2 R package (v.1.38.3).[76] Batch effects were removed using the removeBatchEffect() function (batch = ''sort_batch'') from the limma R package (v.3.54.2).[77]

Mouse bulk RNA-seq data analysis: Differential expression and gene set enrichment

Comparisons of gene expression between sample groups were made using DESeq2 to fit a negative binomial generalized linear model with a group variable. Wald statistics were used to determine the significance of the group coefficient, i.e., the log2-fold change (LFC) in expression between groups. We used the Benjamini-Hochberg method for controlling the false discovery rate (FDR). The p values reported are FDR adjusted. Genes with an adjusted p-value of at most 0.05 were considered differentially expressed (DE) between groups. The LFCs and FDR-adjusted p values were given as input to the fgsea() function from the fgsea R package (v.1.24.0),[78] which implements a preranked gene set enrichment analysis. The rankings of the genes were based on the FDR-adjusted p values. The Gene Ontology Biological Processes (GO-BP) database[79,80] was the gene set used in the enrichment analyses. Enriched pathways (i.e., $p < 0.05$) were collapsed to independent pathways to avoid repetitive terms, using the fgsea collapsePathways() function.

Mouse bulk RNA-seq data analysis: Visualization

All plots illustrating gene expression levels use vst transformed expression. Heatmaps were plotted using the *Heatmap()* function from the ComplexHeatmap R package (v.2.15.1)[81] Heatmaps show the z-scored expression across samples; any values outside the range shown in the numerical legend were squished towards the maximum or minimum values shown.

Mouse single cell RNA-seq data analysis: Quality control and normalization

The unique molecular identifier (UMI) count matrices obtained from the Cell Ranger output were imported into R (v.4.2.2) and processed with the R package Seurat (v. 4.3.0).[82] From this matrix, genes expressed (i.e., having at least one count) in fewer than three cell were removed. TCR related genes were also removed (i.e., genes having the following regex pattern ''∧T[cr][abdgr][vdjgd]([∧*]*)''). Low-quality cells were removed based on the following criteria: 1. Cells with >2.25% mitochondrial percentage were removed, 2. The thresholds for acceptable numbers of detected genes and UMIs per cell were determined by outliers in the joint distribution of unique UMIs and detected genes across cells. Cells with <950 or >3000 detected genes or <2000 or >7500 detected UMIs were discarded were discarded. Further, cells which did not have a corresponding sequenced TCR read where also removed. Overall, 8240 cells passed the above criteria and were used for downstream analysis. To account for differences in sequencing depth across cells, UMI counts were normalized and scaled using regularized negative binomial regression via Seurat's sctransform() function.[83] The resulting normalized counts were used for visualization and clustering downstream analysis.

Mouse single cell RNA-seq data analysis: Clustering and identification of functional cluster markers

We performed principal component analysis (PCA) using the top 3000 highly variable genes. The top 20 principal components for each dataset were used to construct a shared nearest neighbor (SNN) graph and modularity-based clustering using the Louvain algorithm and a cluster resolution of 0.4 as part of the FindClusters() function from the R package Seurat.[82] Uniform manifold approximation and projection (UMAP) visualization was calculated using 20 nearest neighbors for the local approximation of the manifold structure. To determine the functional profile of each cluster, FindAllMarkers() was run with the option ''test.use=LR'', which identifies marker genes by comparing expression of each gene in a cluster against its expression in the rest of the cells using a logistic regression test. Only genes significantly and strongly up regulated in the cluster were considered as potential functional markers.

Mouse single cell RNA-seq data analysis: Identifying expanded clones and enriched motifs

TCRs that did not have exactly one Cdr3a and one Cdr3b sequence were removed. Expanded clones were defined as unique TCRs that were expressed by at least 2 cells. Public clones are a subset of these, which are expressed in at least two samples (i.e., mice). Further, amongst these expanded clones, we found enriched motifs in the Cdr3b sequences of the expanded clones. We first identified lists of all possible k-mers for k=3-8 allowing gaps. We used a Fischer's exact test to determine which k-mers were significantly

enriched in *Ighasec*-/- mice ($P < 0.05$)— where the rows of the test table are condition (i.e., *Ighasec*+/- & *Ighasec*-/-) and the columns are whether the condition contains the motif. The entries than correspond to the number of expanded clones meeting the row and column descriptors.

Mouse single cell RNA-seq data analysis: Visualization

All plots illustrating gene expression levels use SCT transformed expression. Dot plots show the z-scored expression across conditions; any values outside the range shown in the numerical legend were squished towards the maximum or minimum values shown.